Supporting Information

The Synthesis of a Corrole Analog of Aquacobalamin (Vitamin B_{12a}) and its Ligand Substitution Reactions

Caitlin F. Zipp,[a] Joseph P. Michael,[a] Manuel A. Fernandes,[a] Sadhna Mathura,[a] Christopher B. Perry,[a] Isabelle Navizet,[a] Penny P. Govender[b] and Helder M. Marques[a,]*

[a]Molecular Sciences Institute, School of Chemistry, University of the Witwatersrand, PO Wits, Johannesburg, 2050 South Africa and [b]Department of Applied Chemistry, University of Johannesburg, P.O. Box 17011, Doornfontein, Johannesburg, 2028 South Africa

Contents

S1. Figures

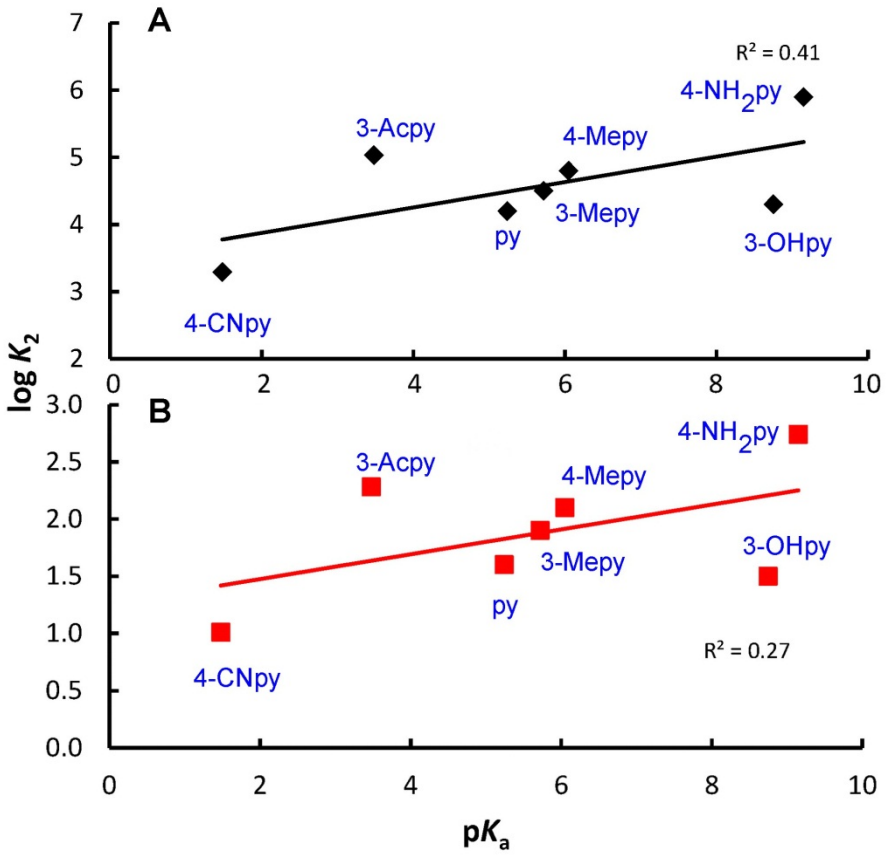

Figure S1. Dependence of (A) log K_1 for coordination by Co(III) corrole **4**, as defined in Table S2.1 of this Supplementary Information, on the pK_a of an entering pyridine ligand. (B) Dependence of log K_2 for coordination by Co(III) corrole **3**, as defined in Table S2.1, on the pK_a of an entering pyridine ligand. The *trans* ligand is py.

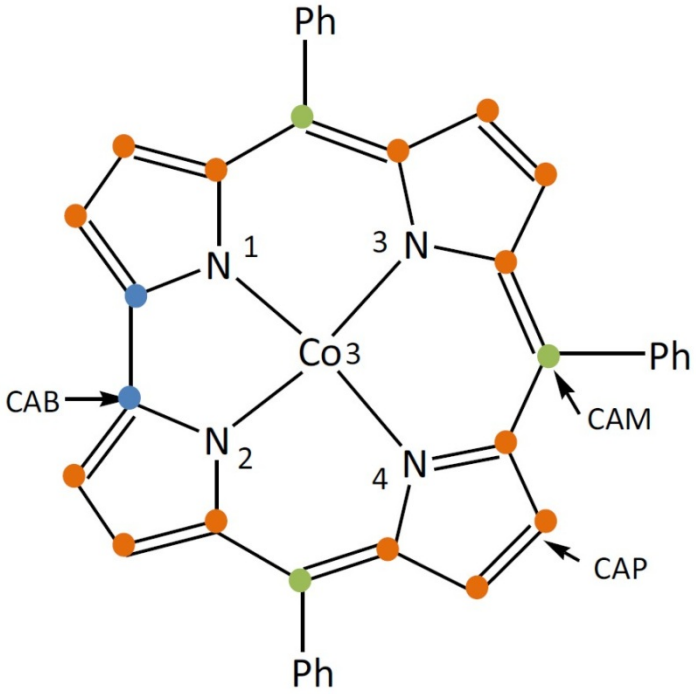

Figure S2. New atom types defined for molecular mechanical calculations of cobalt corroles using GAFF: Co3; the four N-donor nitrogens of the corrole, NC1, NC2, NC3, NC4; CAP (pyrrolic carbon; orange dots); CAM (*meso* carbon, green dots); and CAB (bipyrrole bridge carbons, blue dots).

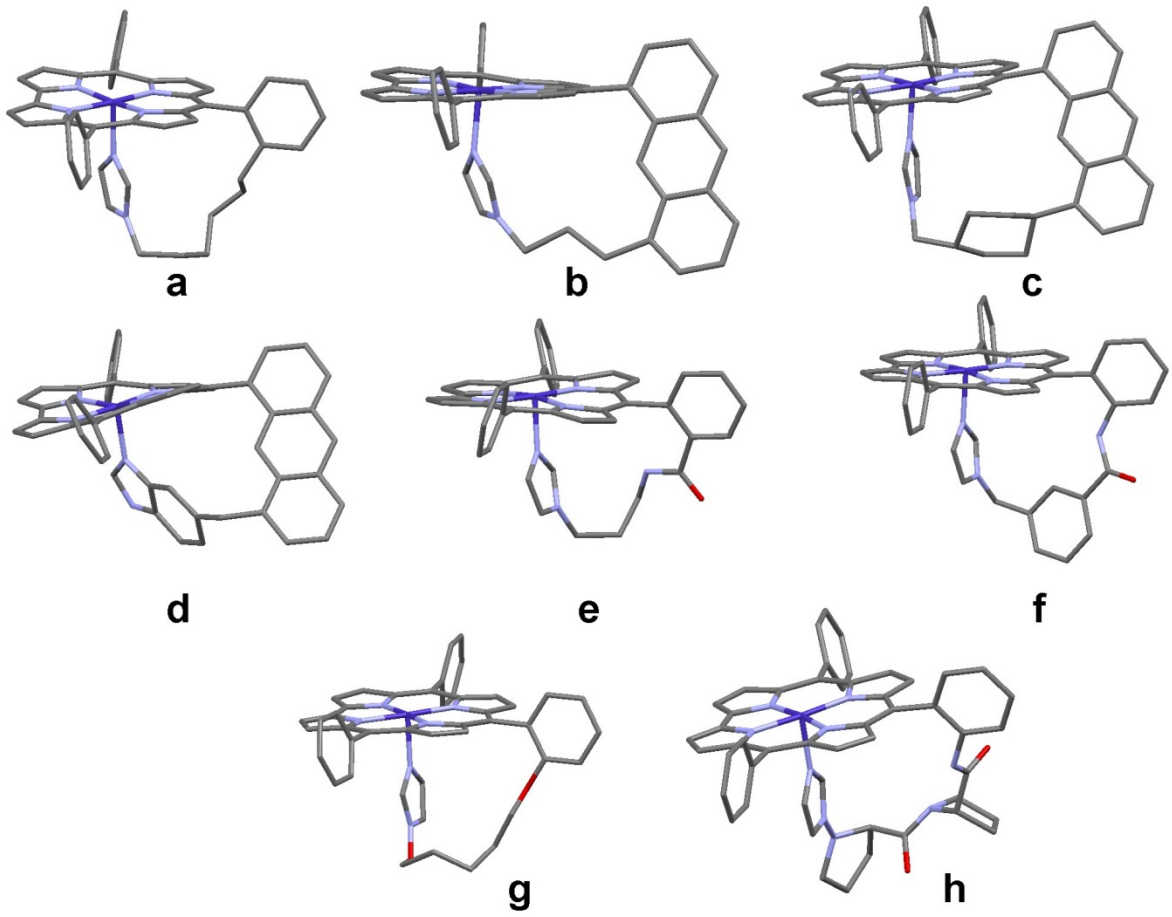

Figure S3. A selection of modelled systems containing (a) a six carbon aliphatic chain, (b) anthracene and a three carbon chain, (c) anthracene and a cyclohexane ring in the chair conformation, (d) anthracene and benzimidazole, (e) an amide and a three carbon chain, (f) an amide and a phenyl ring (meta arrangement), (g) two ethers and a 5 carbon chain, and (h) a proline dipeptide. Hydrogen atoms have been omitted for clarity. Some forty such structures were explored in total. The chosen target was (f).

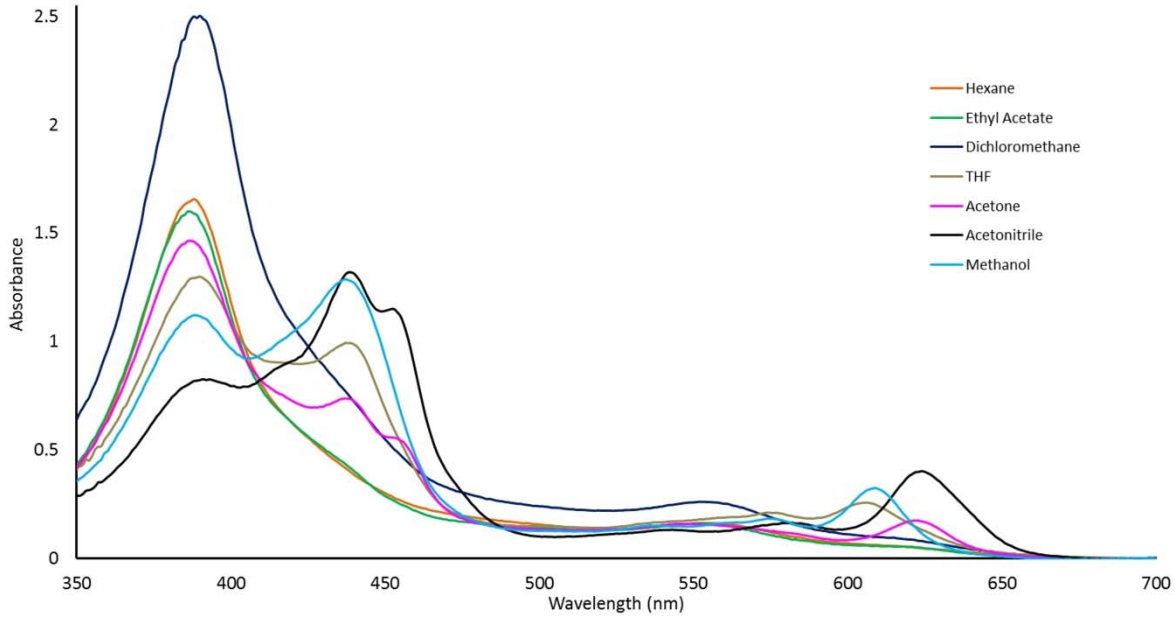

Figure S4. The UV-vis spectra of 50 μM DPTC-Co in a variety of solvents (25 ^{o}C)

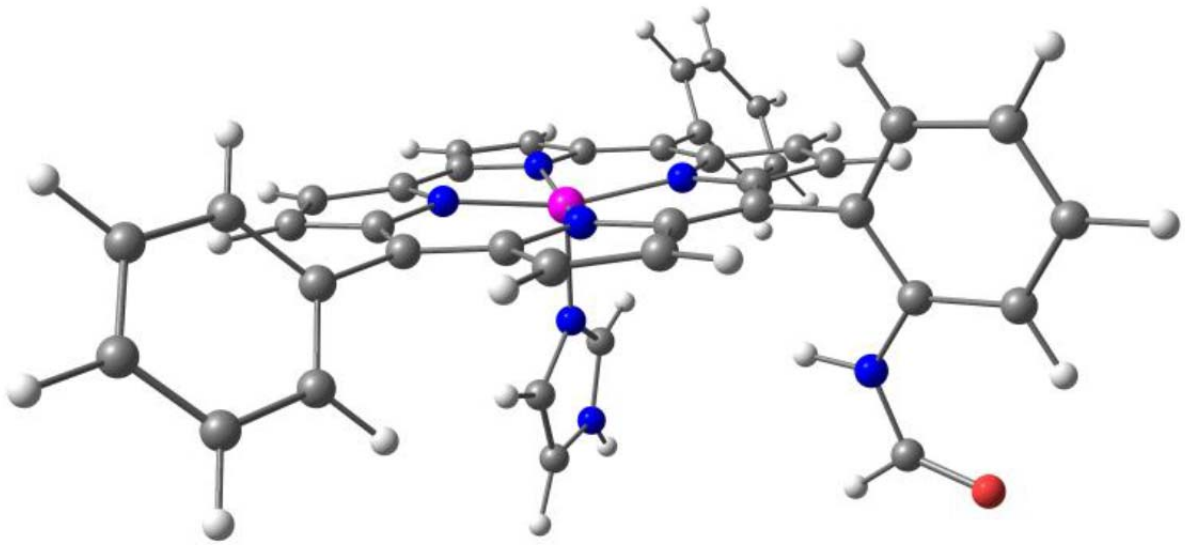

Figure S5. Simplified model of DPTC-Co used for DFT calculations

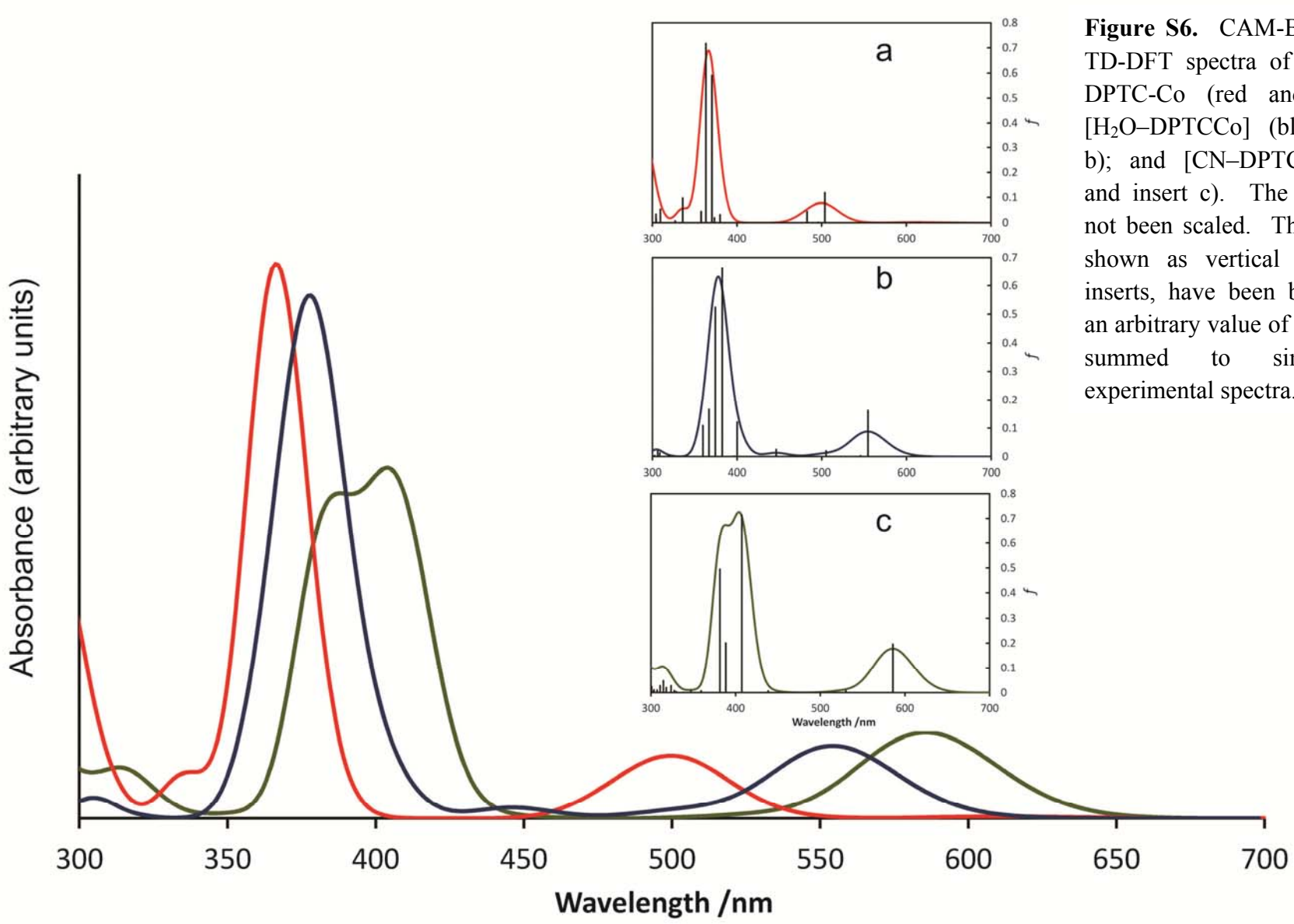

Figure S6. CAM-B3LYP/TZVP TD-DFT spectra of 5-coordinate DPTC-Co (red and insert a); [H_2O–DPTCCo] (blue and insert b); and [CN–DPTCCo]$^-$ (green and insert c). The spectra have not been scaled. The transitions, shown as vertical lines in the inserts, have been broadened by an arbitrary value of 800 cm^{-1} and summed to simulate the experimental spectra.

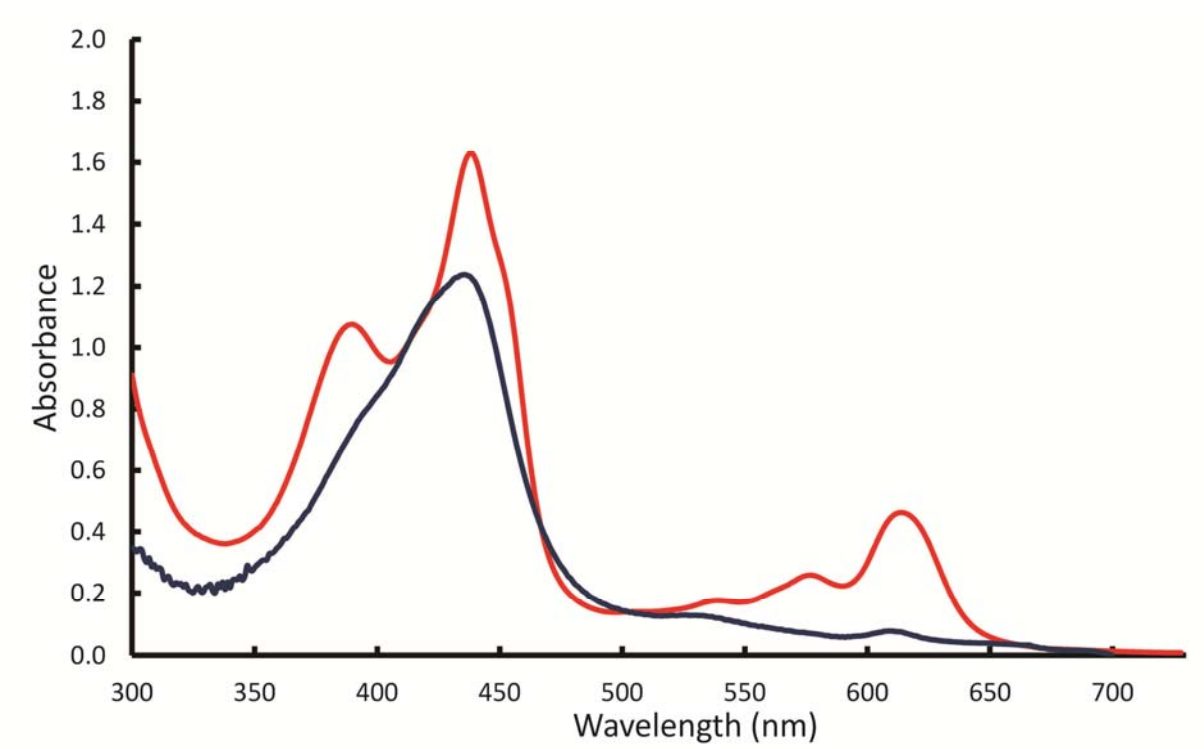

Figure S7. UV-vis spectrum of DPTC-Co in dried methanol (red) and in 80:20 MeOH:H_2O.

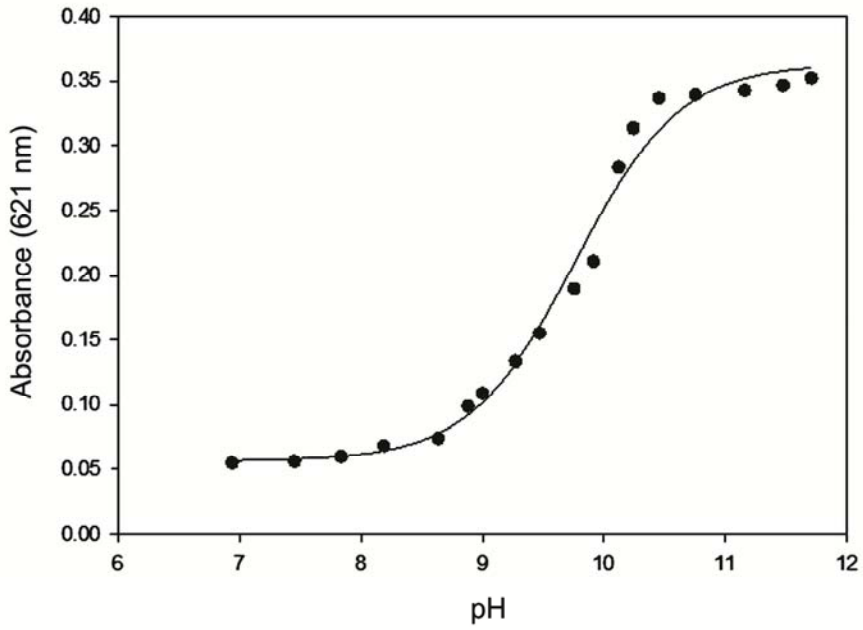

Figure S8. Dependence of the absorbance at 621 nm of [H_2O–DPTC-Co] on pH in 80:20 MeOH:H_2O (μ = 8 mM). The fit gives pK_a = 9.76 ± 0.06.

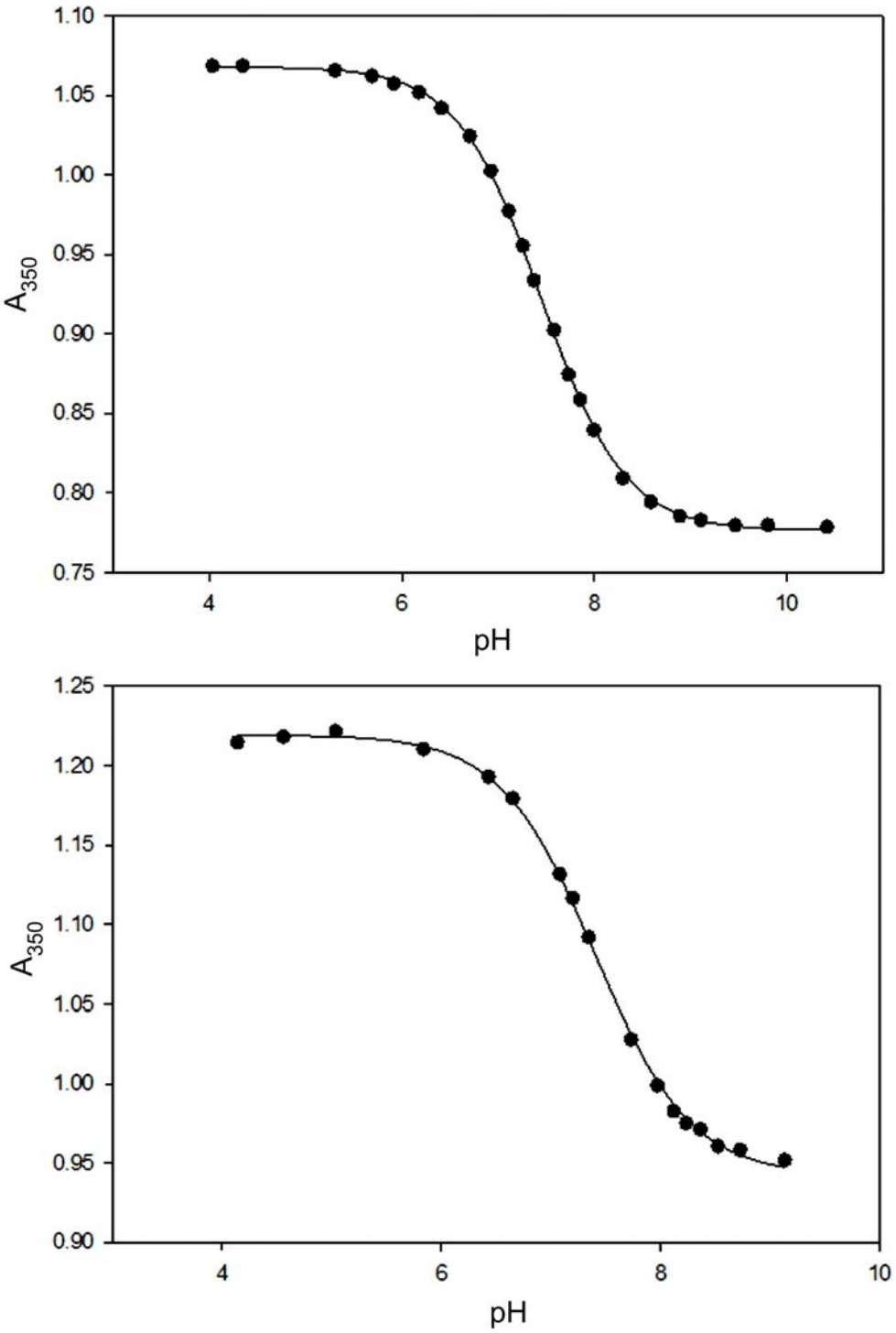

Figure S9. Dependence of the absorbance at 350 nm of H_2OCbl^+ on pH in (top) aqueous solution and (bottom) 80:20 MeOH:H_2O (μ = 8 mM). The fits gives pK_a = 7.462 ± 0.007 and 7.40 ± 0.02, respectively.

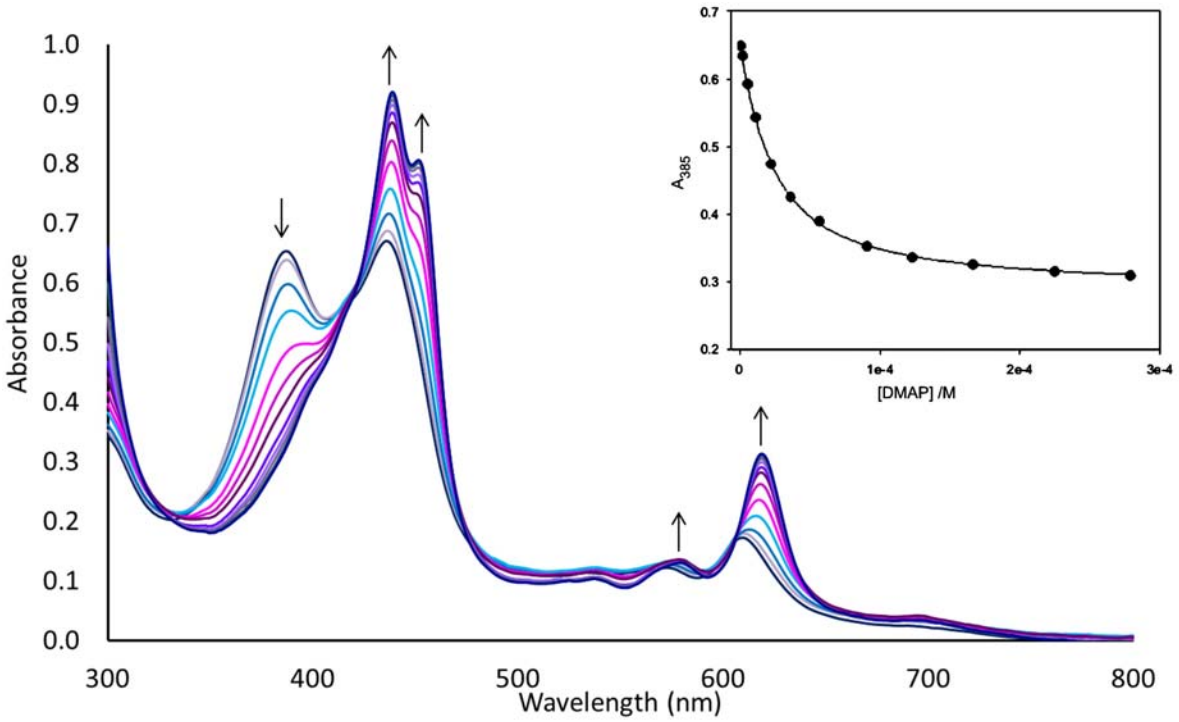

Figure S10. The spectroscopic changes observed on titrating [H_2O–DPTC-Co] in 80% MeO:H_2O (25 ^oC, pH 7, 50 mM MOPS) with DMAP. The insert shows a fit of eqn.3 to the absorbance changes at 385 nm

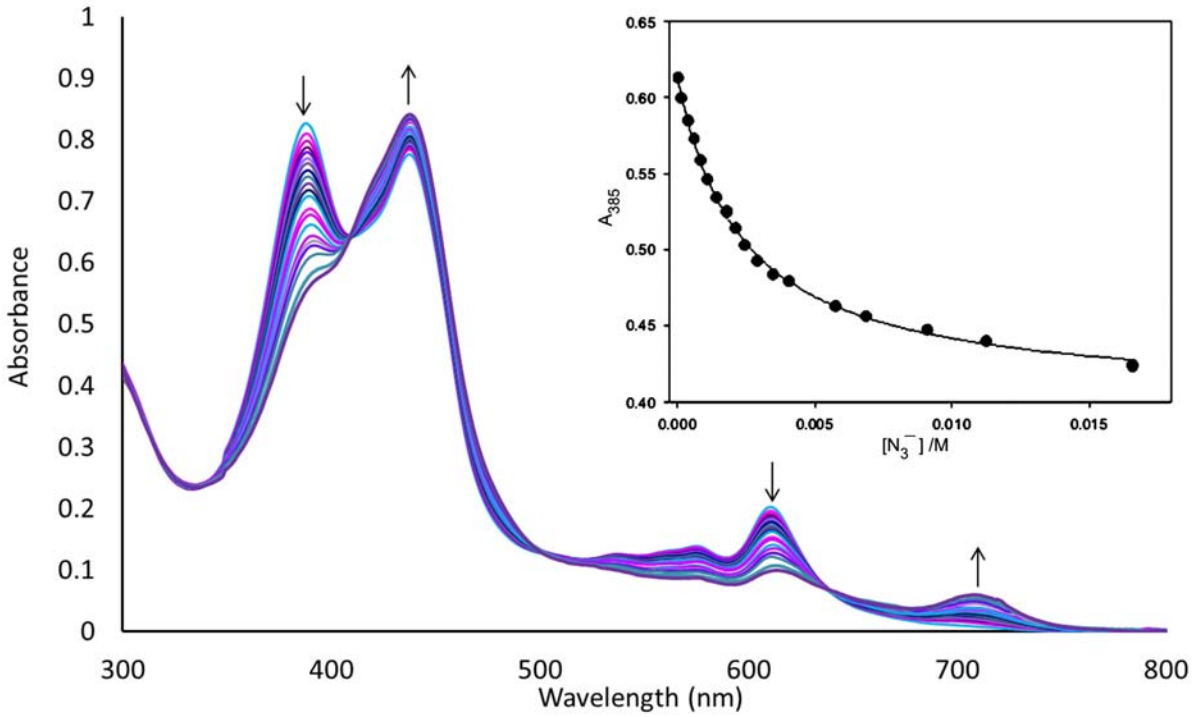

Figure S11. The spectroscopic changes observed on titrating [H_2O–DPTC-Co] in 80% MeO:H_2O (25 ^oC, pH 7, 50 mM MOPS) with N_3^-. The insert shows a fit of eqn.2 to the absorbance changes at 385 nm

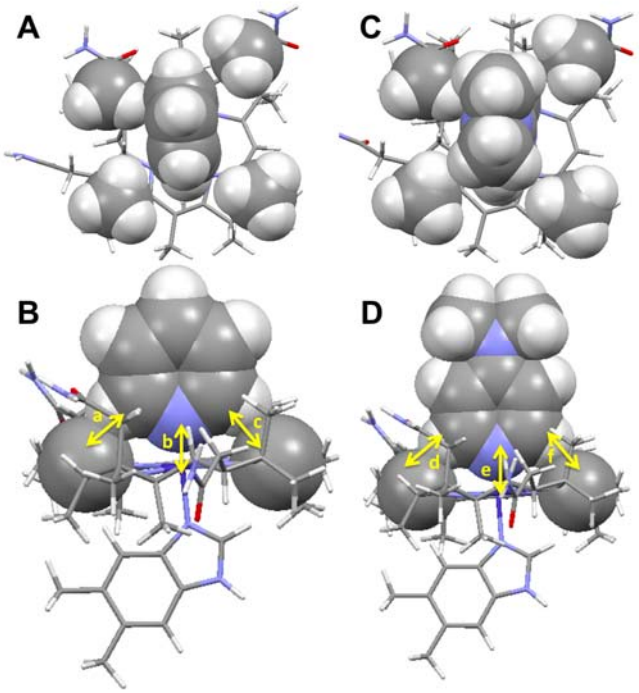

Figure S12. DFT-optimized B_{12} complexes with pyridine (**A** and **B**) and DMAP (**C** and **D**) viewed from the β face and from the side with bond lengths and non-bonded interactions (in Å): a, 2.340; b, 2.045; c, 2.538; d, 2.349; e, 2.027; f, 2.559.

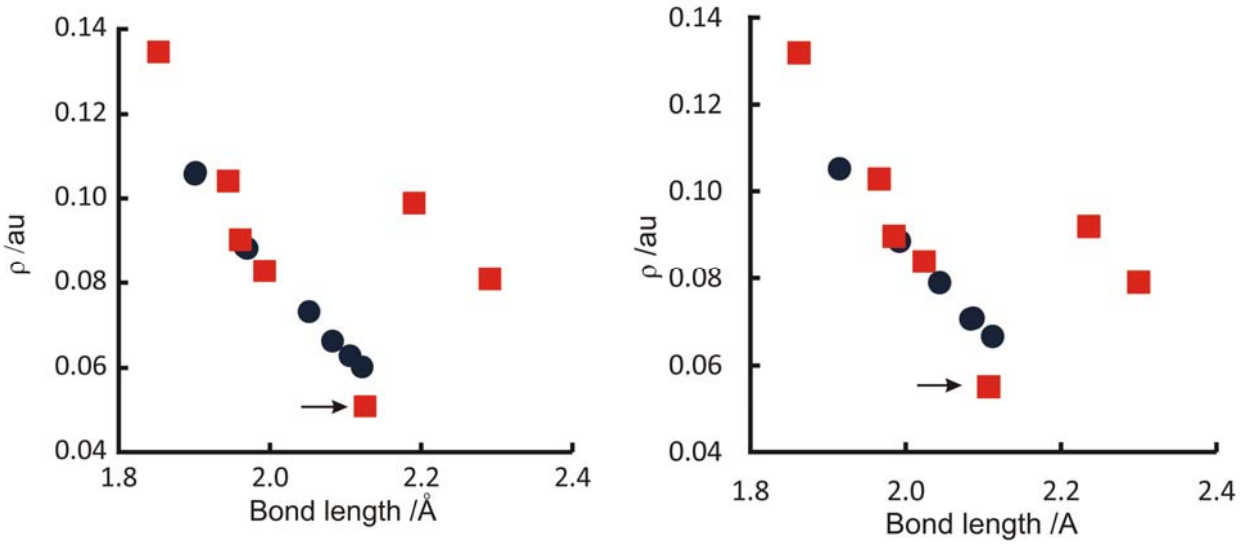

Figure S13. Correlation in (left) DPTC-Co and (right) Co(III) corrin complexes between the axial bond length to the proximal imidazole ligand (●), and the *trans* ligand L (■), and the electron density at the Co–Im and Co–L bond critical points. The two points off the correlation are for ligands with 3rd row donors, TMP and CH_3S^-. The value for the Co–H_2O bond in [H_2O–DPTC-Co] and in the corresponding corrin complex is marked with an arrow.

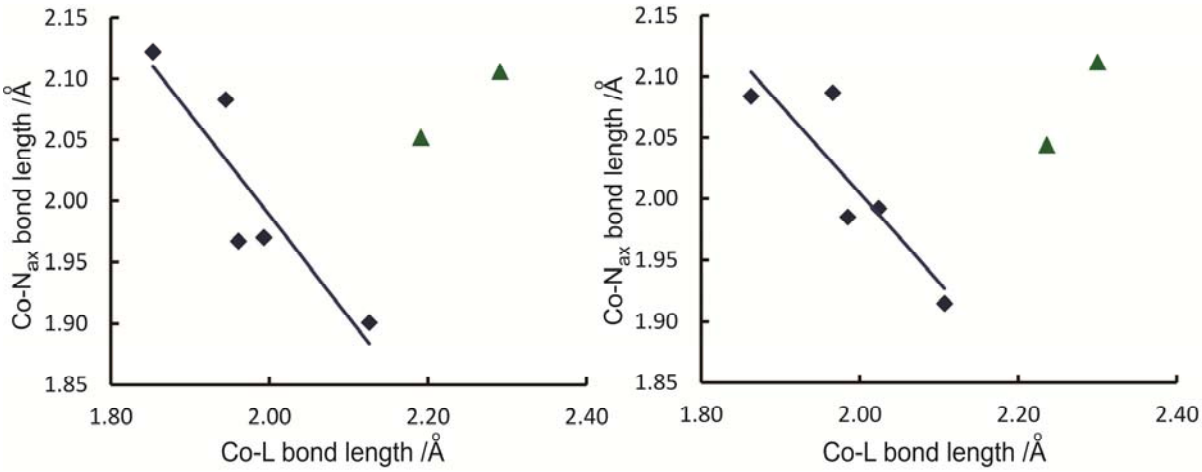

Figure S14. Dependence of the *trans* Co–N_{ax} bond length to imidazole in DFT models of (left) [L–DPTC-Co] and (right) [L–Co(corrin)–Im] on the Co–L bond length. There is a normal *trans* influence (◆) when the donor atom is from the second row (C, N, O) but an apparent inverse *trans* influence (▲) for ligands with a donor atom from the third row (P, S).

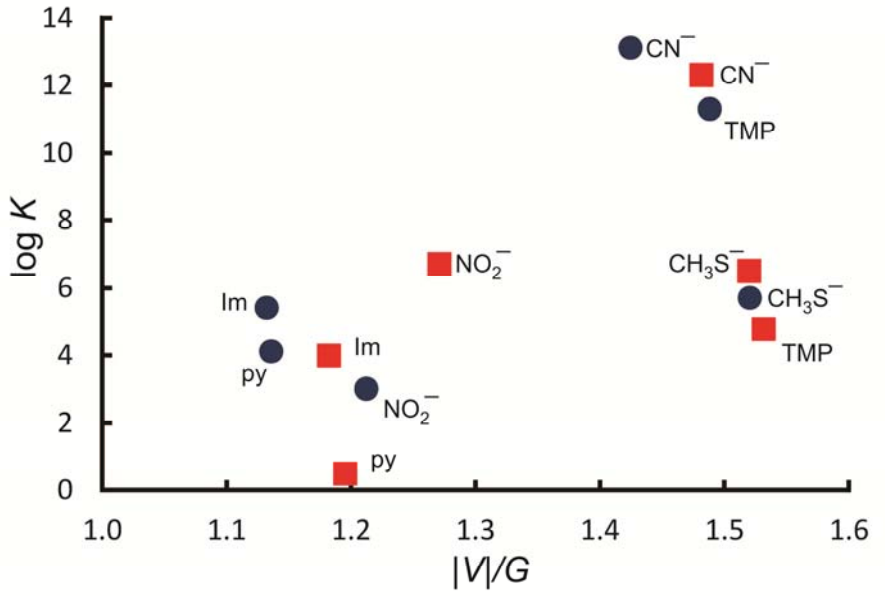

Figure S15. Correlation between $|V|/G$ at the bond critical point of the Co–ligand bond in DFT models (BP86/TZVP) of Co(III) corrole (●) and Co(III) corrin (■) complexes, and the experimentally-determined log *K* values for substitution of axial H_2O. (Imidazole was used as model for *N*-methylimidazole and CH_3S^- as a model for Cys.)

S2. Supplementary Information

S2.1 A brief review of the ligand substitution reactions of Co(III) and Mn(III) corroles.

Equilibrium constants (given as log *K* values) for the coordination of a variety of ligands by Co(III) and Mn(III) corroles (25 ^{o}C) are listed in Table S.2.1.

Table S.2.1. Equilibrium Constants for Coordination of Ligands by Co(III) and Mn(III) Corroles.

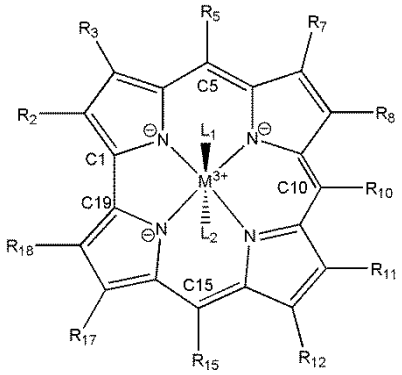

$$L_1\text{–CrI–}L_2 + X \underset{}{\overset{K_1}{\rightleftharpoons}} X\text{–CrI–}L_2 + X \overset{K_2}{\rightleftharpoons} X\text{–CrI–}X$$

M	Corrole[a]	Solvent	X	L_2[b]	log K_1	log K_2	Ref
Co	**1**	PhCN	Cl^-		2.88		1
	3	Acetone	py	py		1.6	2
			4-CNpy	py		1.01	2
			4-NH_2py	py		2.74	2
			4-Mepy	py		2.1	2
			3-Mepy	py		1.9	2
			2-Mepy	py		-0.8	2
			3-Acpy	py		2.28	2
			3-OHpy	py		1.5	2
	4	Acetone	py		4.2	1.6	2
			4-CNpy		3.29	0.82	2
			4-NH_2py		5.9	2.65	2
			4-Mepy		4.8	2.0	2
			3-Mepy		4.5	1.75	2
			2-Mepy		2.0	-1.0	2
			3-Acpy		5.03	2.06	2
			3-OHpy		4.3	1.1	2
	1	CH_2Cl_2	py		4.90	2.10	3,4
	5		py		3.78	2.00	4
	6		py		4.95	2.17	4
	7		py		5.01	2.19	4
	8		py		5.32	2.38	4
	9		py		5.48	2.19	4

M	Corrole[a]	Solvent	X	L_2[b]	log K_1	log K_2	Ref
	11	Benzene	py	PPh_3		2.29	5
	12, y = H		py	PPh_3		1.54	5
	12, y = *p*-OMe		py	PPh_3		1.30	5
	12, y = *p*-Me		py	PPh_3		1.40	5
	12, y = *p*-Cl		py	PPh_3		1.54	5
	12, y = *m*-Cl		py	PPh_3		1.72	5
	12, y = *o*-Cl		py	PPh_3		1.62	5
	1	CH_2Cl_2	CO		4.2		6
	5		CO		3.7		4
	6		CO		4.3		4
	7		CO		3.9		4
	8		CO		4.3		4
	9		CO		4.8		4
Mn	**2**	$CHCl_3$	py		1.17		7
	2	$CHCl_3$	4-Mepy		1.91		7
	2	$CHCl_3$	4-Vnpy		1.17		7
	10	PhCN	$CH_3CO_2^-$		4.5		8
			CN^-		4.7		9
			CNO^-		4.2		9
			Cl^-		4.8		9

Footnotes to Table 1. [a]**1** - $R_5 = R_{15} =$ H; $R_2 = R_3 = R_{17} = R_{18} = R_{10} =$ Ph; $R_7 = R_8 = R_{11} = R_{12} =$ Me; **2** - $R_5 = R_{10} = R_{15} =$ H; $R_2 = R_3 = R_7 = R_8 = R_{11} = R_{12} = R_{17} = R_{18} =$ Me; **3** - $R_5 = R_{10} = R_{15} =$ H; $R_2 = R_3 = R_{17} = R_{18} =$ Me; $R_7 = R_8 = R_{11} = R_{12} =$ Et; **4** - $R_5 = R_{10} = R_{15} =$ H; $R_2 = R_3 = R_7 = R_8 = R_{11} = R_{12} = R_{17} = R_{18} =$ Et; **5** - $R_5 = R_{10} = R_{15} =$ H; $R_2 = R_3 = R_7 = R_{12} = R_{17} = R_{18} =$ Me; $R_8 = R_{11} =$ Et; **6** - $R_5 = R_{15} =$ H; $R_{10} =$ Ph; $R_7 = R_8 = R_{11} = R_{12} =$ Me; $R_2 = R_3 = R_{17} = R_{18} =$ *p*-OMePh ; **7** - $R_5 = R_{10} = R_{15} =$ H; $R_2 = R_3 = R_{17} = R_{18} =$ Ph; $R_7 = R_{12} =$ Me; $R_8 = R_{11} =$ Et; **8** - $R_5 = R_{15} =$ H; $R_{10} =$ Ph; $R_7 = R_8 = R_{11} = R_{12} =$ Me; $R_2 = R_3 = R_{17} = R_{18} =$ *o*-OMePh; **9** - $R_5 = R_{15} =$ H; $R_2 = R_3 = R_7 = R_{12} = R_{17} = R_{18} = R_{10} =$ Ph; $R_8 = R_{11} =$ Me; **10** - $R_5 = R_{15} =$ Mes; $R_{10} =$ Ph; $R_2 = R_3 = R_7 = R_8 = R_{11} = R_{12} = R_{17} = R_{18} =$ H; **11** - $R_5 = R_{10} = R_{15} =$ H; $R_2 = R_3 = R_7 = R_8 = R_{11} = R_{12} = R_{17} = R_{18} =$ Me; **12** - $R_5 = R_{10} =$ R15 = *y*-Ph; $R_2 = R_3 = R_7 = R_8 = R_{11} = R_{12} = R_{17} = R_{18} =$ Me. [b]In all cases L_1 is either a solvent molecule (if the reaction occurs in a coordinating solvent) or that coordination site is vacant. If L_2 is not explicitly given, either the coordination site of the metal is vacant or L_2 is a solvent molecule. If both log K_1 and log K_2 are given, then $L_1 = X$.

The equilibrium constants tend to increase with the basicity of the entering ligand, X, as is evident from log K_2 values for the coordination of substituted pyridines *trans* to py itself Table S.2.1), although the correlations are weak (see Figure S1 of this Supporting Information). A substituent next to the coordinating N of a pyridine decreases the stability constant markedly, as evidenced by a low log K for coordination of 2-Mepy. For coordination of pyridines by the Co(III) corrole **4** as defined in Table S.2.1, log K_1 > log K_2; the *trans* ligand therefore markedly affects the value of the stability constant. The value of log K_1 depends on the substituents on the periphery of the corrole ring in Co(III) corroles (corroles **1**, **5-9**,Table 1). The presence of aliphatic substituents at the β positions and H at the *meso* positions on the corrole ring leads to a relatively low stability constant for the coordination of pyridine (**5**, log K_1 = 3.78). The addition of Ph to the C10 *meso* position increases log K_1 (**1**, **6,** log K_1 = 4.90 and 4.95, respectively), and the presence of Ph at six of the eight β positions, and on C10, increases log K_1 to 5.48.

The *cis* influence of the corrole was investigated in a series of Co(III) corroles bearing Me at the β positions and phenyl groups with different substituents at the *meso* positions (the corroles **12**). The effect is small with log K_2 values for coordination of pyridine *trans* to PPh_3 varying by at most 0.42 units. CO has an affinity for Co(III) corroles comparable to that of pyridine, while Mn(III) corroles have a somewhat lower affinity for pyridine than Co(III) corroles. Anionic ligands bind strongly to Mn(III) corroles (log $K_1 > 4$). Chloride has a considerably higher affinity for a Mn(III) corrole than a Co(III) corrole (log $K_1 = 4.8$ and 2.88, respectively).

S2.2 Attempted synthesis of an aldehyde bearing the tail motif

Collman's synthesis of an imidazole acid chloride for the synthesis of a biomimetic metalloporphyrin system[10] was the basis of the envisaged preparation of an aldehyde bearing the required tail motif (Scheme S1).

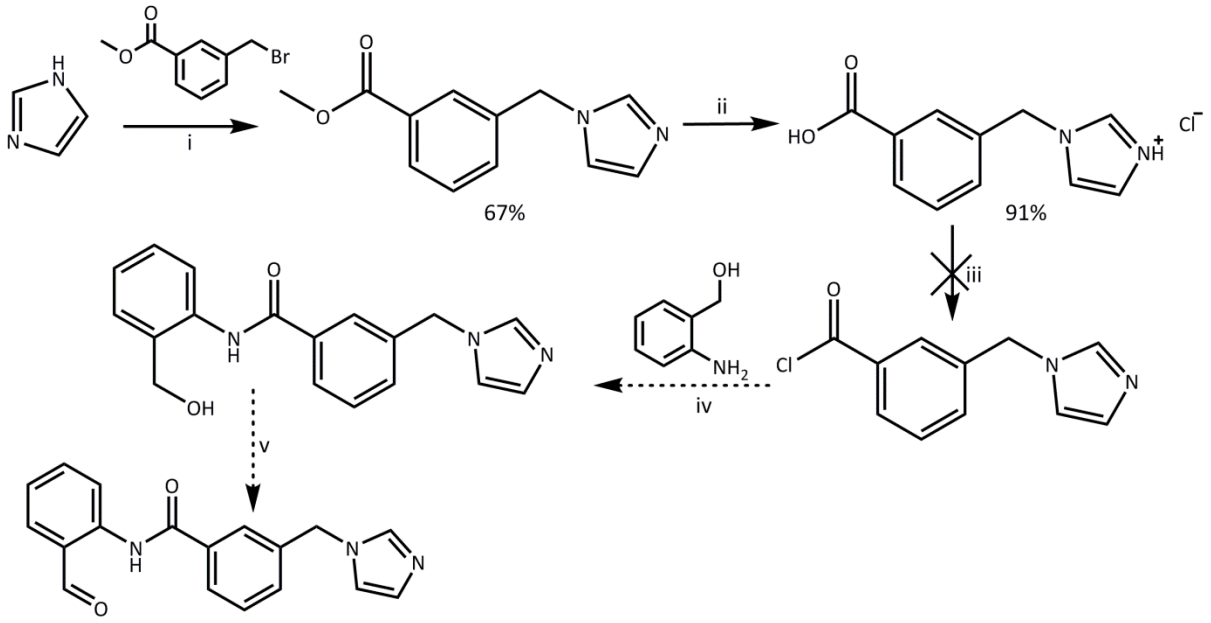

Scheme S1. Attempted synthesis of the tailed aldehyde with the preparation of an acid chloride based on Collman's synthesis.[10] i) DMF, 8 hrs; ii) HCl (32%), reflux, 2 hrs; iii) CH_3CN (dry, degassed), oxalyl chloride, reflux, 1 hr; iv) CH_2Cl_2 (dry), triethylamine, 0°C, 10 min, then room temperature, 2 hrs; v) MnO_2, $CHCl_3$, 20 hrs.

Imidazole was treated with methyl 3-(bromomethyl)benzoate in DMF. The product, methyl 3-(1*H*-imidazol-1-ylmethyl)benzoate, was isolated as a yellow oil in 67% yield. ^{1}H NMR spectroscopic analysis showed the presence of imidazole protons at 7.58, 7.10 and 6.92 ppm, and aromatic protons at 8.00, 7.88, 7.44 and 7.33 ppm, as well as the bridging methylene protons at 5.17 ppm and the methoxy protons at 3.91 ppm. The parent ion was present in the mass spectrum at m/z = 217.32 ($[M+H]^+$).

Hydrolysis of the ester was achieved by refluxing in 32% hydrochloric acid for 2 hours. The resultant white powder, isolated as the hydrochloride salt of the free carboxylic acid in 91% yield, crystallised in the $P2_1/c$ space group from methanol and hexane. ^{1}H NMR spectroscopic analysis indicated the loss of the methoxy protons as well as a down-field shift of the imidazole protons from 7.58, 7.10 and 6.92 ppm to 9.18 and 7.76-7.66 ppm, consistent with the presence of a charged imidazole species. ^{13}C NMR spectroscopic analysis indicated

a shift in the position of the carbonyl carbon from 166.45 ppm in the ester to 168.91 ppm in the acid. The parent ion (with the chloride counter-ion) was present in the mass spectrum at m/z = 237.15 ($[M+H]^+$). The crystallographic details of the acid chloride are given in Table S2.4.1.

We were unable to prepare the acid chloride from the carboxylic acid, despite many attempts. Various factors were investigated, including solvent, chlorinating agent (oxalyl chloride and thionyl chloride) and base (organic, inorganic and an ion exchange resin were used). The use of a coupling agent (1,1'-carbonyldiimidazole) was also unsuccessful.

S2.3 The synthesis of DPTC-Co

Materials and purification methods. Reagents and solvents were used as received unless otherwise indicated. 2-Aminobenzyl alcohol, benzaldehyde, 1,1′-carbonyldiimidazole (CDI), Dess-Martin periodinane (DMP), 2,3-dichloro-5,6-dicyano-1,4-benzoquinone (DDQ), methyl 3-(bromomethyl)benzoate, 4-methylimidazole, *o*-nitrobenzaldehyde, *p*-chloranil, pyridine, pyridinium chlorochromate (PCC), pyrrole and phenol were from Aldrich; 2-aminophenol, cobalt(II) acetate, imidazole, oxalyl chloride, *p*-methoxy benzaldehyde, thionyl chloride and triphenylphosphine were from Merck; benzoyl chloride (distilled), boron trifluoride diethyl etherate, manganese(IV) oxide, trifluoroacetic acid were from Sigma-Aldrich; 3-(chloromethyl)benzoyl chloride was from Acros Organic; *p*-nitrobenzaldehyde was from BDH; triethylamine was from SAARChem (South Africa); and γ-butyrolactone was from SMM Chemicals (South Africa).

3-(Chloromethyl)-N-[2-(hydroxymethyl)phenyl]benzamide. 3-(Chloromethyl)benzoyl chloride (0.71 ml, 5 mmol) and 2-aminobenzyl alcohol (0.615 g, 5 mmol) were added to dry dichloromethane (15 mL). Freshly distilled triethylamine (0.767 ml, 0.557 g, 5.5 mmol) was added dropwise to the reaction mixture at 0°C. The solution was stirred at 0°C for 10 minutes and then at room temperature for 2 hours. Water was added and the organic layer was separated, dried over Na_2SO_4 and the solvent was removed *in vacuo*. The crude product was purified by column chromatography on flash silica gel with hexane: ethyl acetate (1:1 v/v) as eluent. The desired product was obtained as an off-white solid (0.793 g, yield 58%). MP 98-99°C, ^{1}H (300 MHz, $CDCl_3$) δ (ppm): 9.70 (s, 1H, NH), 8.21 (d, J = 8.0 Hz, 1H, H6), 7.92 (s, 1H, H2′), 7.81 (d, J = 7.8 Hz, 1H, H6′), 7.56 (d, J = 7.8 Hz, 1H, H3), 7.44 (dd, J = 9.5, 5.9 Hz, 1H, H4 or H5), 7.37-7.29 (m, 1H, H4 or H5), 7.15 (dd, J = 7.5, 1.4 Hz, 1H, H4′), 7.06 (td, J = 7.4, 1.1 Hz, 1H, H5′), 4.75 (d, J = 5.8 Hz, 2H, CH_2OH), 4.61 (s, J = 4.8 Hz, 2H, CH_2Cl), 3.00 (t, J = 5.8 Hz, 1H, OH). ^{13}C (75 MHz, $CDCl_3$) δ (ppm): 165.02 (C=O), 138.28 (C1, C2, C1′ or C3′), 137.73 (C1, C2, C1′ or C3′), 135.18 (C1, C2, C1′ or C3′), 131.95 (C1, C2, C1′ or C3′), 129.40 (C_{ar}), 129.24 (C_{ar}), 129.15 (C_{ar}), 128.66 (C_{ar}), 127.53 (C_{ar}), 126.80 (C_{ar}), 124.38 (C_{ar}), 122.18 (C_{ar}), 64.80 (CH_2OH), 45.62 (CH_2Cl). HRMS (EI) *m/z*: 275.0702 ($[M]^+$); calc.: 275.0713.

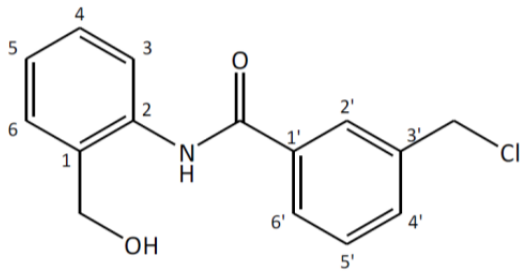

ν_{max} (cm^{-1}): 3217 (m, br, O–H stretch); 3028 (w, N–H stretch); 1740, (very s, C=O); 1653 (s, N–H bend) 747 (s, C–Cl stretch).

N-[2-(Hydroxymethyl)phenyl]-3-(1H-imidazol-1-ylmethyl)-benzamide.[11] 3-(Chloromethyl)-*N*-[2-(hydroxymethyl)phenyl]benzamide (4.183 g, 15.17 mmol) and imidazole (10.329 g, 0.52 mol) in DMF (15 mL) were stirred at room temperature for 20 hours. The reaction was diluted with water (100 mL) and extracted into dichloromethane (3 × 100 mL). The combined organic fractions were extracted into a hydrochloric acid solution (10%, 3 × 100 mL). The acidic solution was neutralised with ammonia solution, becoming cloudy. The product was extracted into cholroform (3 × 50 mL) and washed with water (6 × 100 mL) to remove any DMF present. The solution was then dried over Na_2SO_4 and the solvent was removed *in vacuo* to yield a yellow solid (3.723 g, yield 80%). MP 144-146°C. ^{1}H (300 MHz, MeOD) δ (ppm): 7.92-7.77 (m, 4H, H3, H4, H5 & H6), 7.53 (t, J = 7.6 Hz, 1H, H5′), 7.47 (d, J = 7.8 Hz, 1H, H6′), 7.38 (d, J = 7.5 Hz, 1H, $H4_{imid}$), 7.33 (td, J = 7.8, 1.5 Hz, 1H, H4′), 7.20 (td, J = 7.5, 1.1 Hz, 1H, $H5_{imid}$), 7.16 (s, 1H, H2′), 7.00 (s, 1H, $H2_{imid}$), 5.33 (s, 2H, $C\underline{H}_2OH$), 4.71 (s, 2H, $CH_{2\ imid}$). ^{13}C (75 MHz, MeOD) δ (ppm): 166.04 (C=O), 137.76 ($C_{2\ imid}$), 136.13 (C1, C2, C1′ or C3′), 134.94 (C1, C2, C1′ or C3′), 132.96 (C1, C2, C1′ or C3v), 130.64 (C1, C2, C1′ or C3′), 128.97 (C_{ar}), 128.00 (C_{ar}), 127.78 (C_{ar}), 127.66 (C_{ar}), 126.38 (C_{ar}), 126.24 (C_{ar}), 126.19 (C_{ar}), 124.98 (C_{ar}), 123.25 ($C_{4\ imid}$), 119.42 ($C_{5\ imid}$), 62.00 (CH_2OH), 49.66 ($CH_{2\ imid}$). HRMS (EI) *m/z*: 307.1316 ($[M]^+$); calc.: 307.1321. ν_{max} (cm^{-1}): 3028 (m, very broad, O–H stretch and N–H stretch); 1739 (m, C=O stretch); 1664 (s, N–H bend); 1619 (m, C=N stretch).

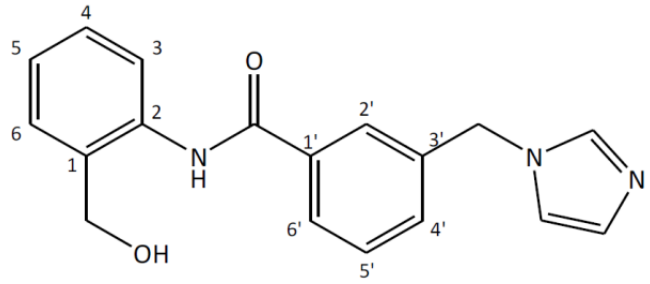

N-(2-Formylphenyl)-3-(1H-imidazol-1-ylmethyl)benzamide. *N*-[2-(Hydroxymethyl)phenyl]-3-(1*H*-imidazol-1-ylmethyl)benzamide (0.7633 g, 2.5 mmol) and manganese(IV) oxide (4.347 g, 50 mmol) were stirred in chloroform (50

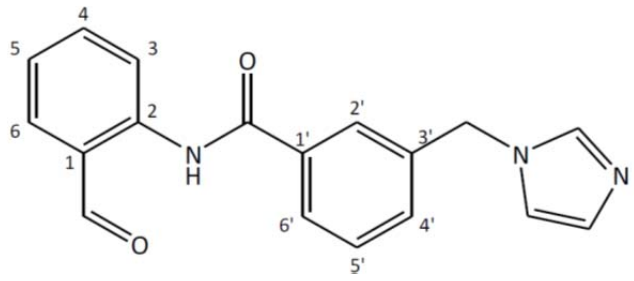

mL) for 20 hours. The reaction mixture was filtered through celite with chloroform as eluent. The solvent was removed *in vacuo*. The oily residue crystallised when placed under high vacuum. The off-white solid was recrystallised from methanol and hexane (0.7225 g, 95%). MP 149-150°C. ^{1}H (300 MHz, $CDCl_3$) δ (ppm): 12.11 (s, 1H, CHO), 10.00 (s, 1H, NH), 8.90 (d, J = 8.5 Hz, 1H, H3), 8.00 (d, J = 7.7 Hz, 1H, H6), 7.92 (s, 1H, $H2_{imid}$), 7.77 (d, J = 7.6 Hz, 1H, H6′), 7.68 (t, J = 7.9 Hz, 1H, H4 or H5), 7.63 (s, 1H, H2′), 7.54 (t, J = 7.7 Hz, 1H, H4′ or H5′), 7.37 (t, J = 8.0 Hz, 1H, H4 or H5), 7.30 (t, J = 7.5 Hz, 1H, H4′ or H5′), 7.10 (d, J = 0.7 Hz, 1H, $H4_{imid}$), 6.99 (d, J = 0.9 Hz, 1H, $H5_{imid}$), 5.25 (s, 2H, CH_2). ^{13}C (75 MHz, $CDCl_3$) δ (ppm): 195.98 (CHO), 165.37 (C=O amide), 140.89 (C2), 137.29 ($C2_{imid}$), 136.35 (C1, C1′ or C3′), 136.22 (C1, C1′ or C3′), 135.12 (C1, C1′ or C3′), 130.86 (C_{ar}), 130.00 (C_{ar}), 129.61 (C_{ar}), 126.94 (C_{ar}), 126.72 (C_{ar}), 123.31 (C_{ar}), 121.98 (C_{ar}), 119.81 ($C4_{imid}$), 119.26 ($C5_{imid}$), 50.42 (CH_2). HRMS (EI) *m/z*: 305.1164 ([M]+); calc.: 305.1164. ν_{max} (cm^{-1}): 3458 (w, N–H stretch); 1738 (s, C=O stretch); 1659 (m, C=N stretch); 1286 (C–N stretch).

10-(2-[[4-(1H-Imidazol-1-ylmethyl)benzoyl]amino]phenyl)-5,15-diphenylcorrole, DPTC. 2,2′-(Phenylmethylene)bis(1*H*-pyrrole) (1.112 g, 5 mmol) and 3′-(1*H*-imidazol-1-ylmethyl)-*N*-(2-formylphenyl)benzamide (0.763 g, 2.5 mmol) were dissolved in methanol (150 mL). Hydrochloric acid (32%, 7.5 mL) in water (150 mL) was added to the reaction flask which

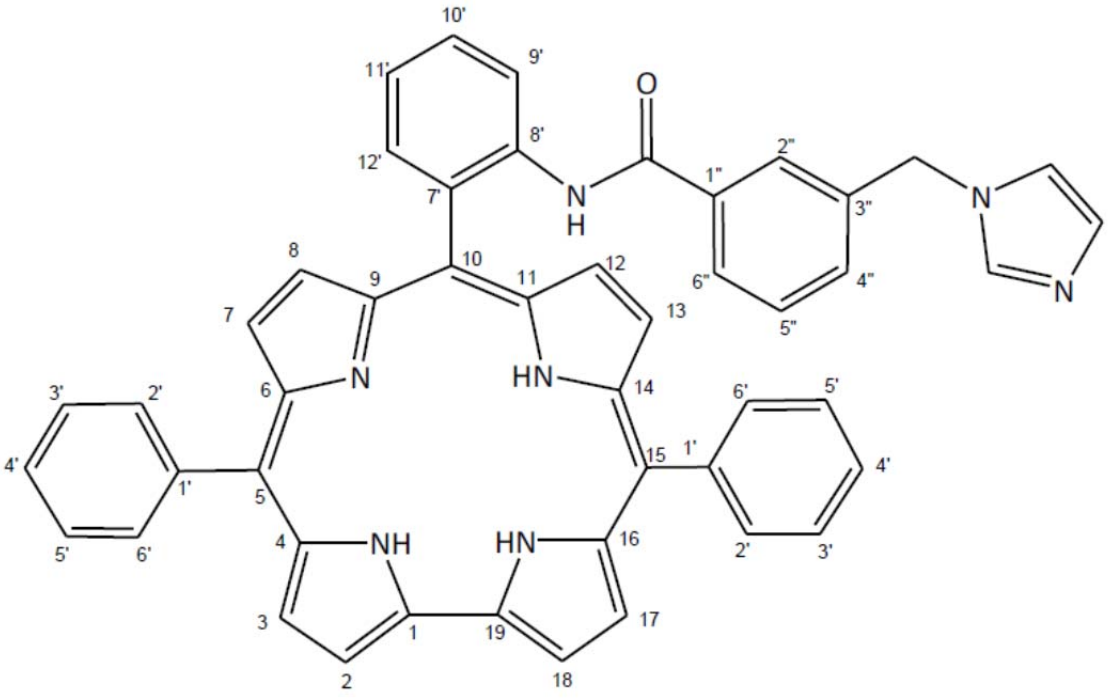

was stoppered and kept in the dark. The reaction mixture was stirred at ambient temperature for 1 hour and then extracted into chloroform. The organic layer was washed with water

twice, dried with Na_2SO_4 and diluted with chloroform to a volume of 500 mL. *p*-Chloranil (1.000 g, 4 mmol) was added and the reaction mixture was stirred for 6 hours in the dark. The black reaction mixture was concentrated *in vacuo*. The crude product mixture was separated by column chromatography on flash silica gel with hexane:ethyl acetate (1:1 v/v) as eluent. The corrole-containing fractions (identified using UV-vis spectroscopy) were combined and evaporated to dryness *in vacuo* and a dark green solid was obtained (0.1911 g, yield 10.5%). MP > 250°C. ^{1}H (500 MHz, $CDCl_3$) δ (ppm): 9.04 (d, J = 8.3 Hz, 1H, NH), 8.85 (t, J = 3.5 Hz, 2H, pyrrole H$_\beta$), 8.83 (d, J = 4.6 Hz, 2H, pyrrole H$_\beta$), 8.46 (d, J = 4.0 Hz, 2H, pyrrole H$_\beta$), 8.40 (d, J =4.6 Hz, 2H, pyrrole H$_\beta$), 8.34 (d broad, 4H, H2′ & H6′), 8.26 (s, 1H, H2$_{imid}$), 7.80 (t, J = 7.3 Hz, 6H, H3′, H4′ & H6′), 7.71 (d, J = 7.4 Hz, 2H, H$_{ar}$), 7.70-7.65 (m, 1H, H$_{ar}$), 7.76 (s, 1H, H2″), 7.43 (t, J = 7.3 Hz, 1H, H$_{ar}$), 7.09 (t, J = 7.7 Hz, 1H, H2″), 6.77 (d, J = 7.3 Hz, 1H, H5$_{imid}$), 3.90 (s, 2H, CH_2) 1.20 (s broad, 3H, 3 × NH). ^{13}C (126 MHz, CDCl3) δ (ppm): 163.61 (C=O), 143.52, 140.73, 140.09, 138.04, 137.56, 136.07, 136.01, 135.86, 135.29, 135.13, 133.86, 131.77, 131.21, 130.49, 129.03, 128.98, 128.94, 128.66, 128.50, 128.14, 127.95, 127.41, 126.02, 125.84, 123.14, 122.73, 121.14, 120.91, 119.77, 117.18, 116.49, 114.59, 112.71, 111.16, 101.89, 21.03 (CH_2). LRMS (ESI) *m/z:* 726 ($[M+H]^+$); calc.: 726. ν_{max} (cm^{-1}): 2964, 2927, 2862 (m, N–H stretch); 1737 (w, C=O stretch); 1085 (s, broad, aromatic out of plane bend).

[10-(2-[[4-(1H-Imidazol-1-ylmethyl)benzoyl]amino]phenyl)-5,15-diphenylcorrolato]-cobalt(III), DPTC-Co. 10-(2-[[4-(1*H*-Imidazol-1-ylmethyl)benzoyl]amino]phenyl)-5,15-diphenylcorrole (0.191 g, 0.263 mmol) was dissolved in methanol (200 mL). Cobalt(II) acetate (10 mol equiv, 0.656 g, 2.633 mmol) and sodium acetate (10 mol equiv, 0.358 g, 2.633 mmol) were added and the reaction mixture was heated at reflux for two hours with the round bottomed flask covered in foil. The reaction mixture was concentrated *in vacuo* upon cooling to room temperature. The solid was dissolved in ethyl acetate and washed with water (three times) and concentrated *in vacuo* to give a black solid (0.176 mg, yield 85.5%). MP > 250°C. ^{1}H (500 MHz, $CDCl_3$) δ (ppm): 8.96 (d, J = 8.4 Hz, 1H, NH), 8.80 (d, J = 4.1 Hz, 2H, pyrrole H$_\beta$), 8.40 (d, J = 4.0 Hz, 4H, pyrrole H$_\beta$), 8.19-8.10 (m, 5H, pyrrole H$_\beta$ and H$_{ar}$), 8.01 (d, J = 4.0 Hz, 2H, H$_{ar}$), 7.94 (d, J = 7.2 Hz, 1H, H2$_{imid}$), 7.88 (d, J = 7.7 Hz, 1H, H2″), 7.73 (d, J = 12.5 Hz, 6H, H$_{ar}$), 7.65 (d, J = 6.0 Hz, 3H, H$_{ar}$), 7.35 (t, J = 7.3 Hz, 2H, H$_{ar}$), 7.20 (t, J = 7.7 Hz, 2H, H$_{ar}$), 6.78 (d, J = 7.3 Hz, 1H, H$_{ar}$), 3.99 (s, 2H, CH_2). ^{13}C (126 MHz, CDCl3) δ (ppm): 163.08 (C=O), 154.09; 153.19; 150.71; 148.22; 147.59; 142.76; 139.29; 139.18; 136.61; 135.50; 135.43; 134.19; 134.01 (quaternary C), 130.06 (pyrrole C$_\beta$), 129.84 (pyrrole

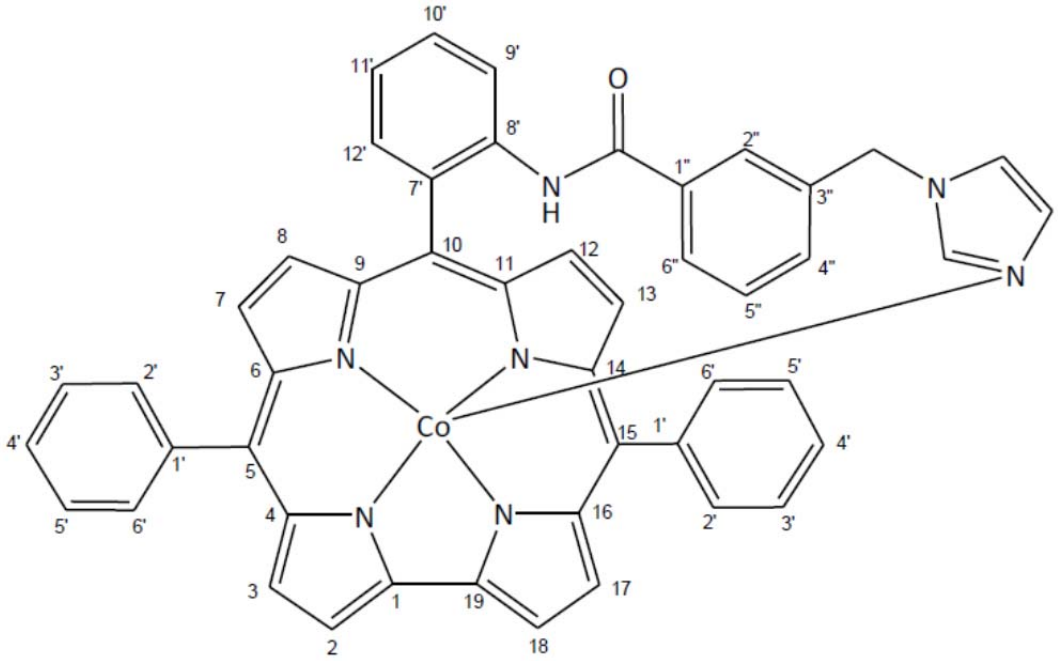

C_{β}), 129.74, 129.61, 129.59, 129.36, 129.04, 128.84, 128.29, 128.14, 127.70, 127.55, 126.78, 126.16, 125.75, 124.81, 123.28, 122.31, 120.63 (pyrrole C_{β}), 119.83 (pyrrole C_{β}), 118.96, 118.25, 114.07, 49.98 (CH_2). LRMS (APCI) *m/z*: 782.4 ($[M+H]^+$); calc.: 782.2. ν_{max} (cm^{-1}): 3406 (w, N–H stretch); 1673 (s, C=O stretch); 1578, 1518 (C=N stretch); 1441 (C–N stretch); 1051, 1012, 983 (s, aromatic out of plane bend).

S2.4 Molecular structures

Table S2.4.1. Crystal data and structure refinement for 3-(chloromethyl)-*N*-[2-(hydroxymethyl)phenyl]-benzamide

CCDC deposition code	CCDC 980627	
Empirical formula	C_{15} H_{14} Cl N O_2	
Formula weight	275.72	
Temperature	173(2) K	
Wavelength	0.71073 Å	
Crystal system	Monoclinic	
Space group	$P2_1/n$	
Unit cell dimensions	a = 4.1955(2) Å	α= 90°
	b = 26.0540(15) Å	β = 90.279(2)°
	c = 12.1996(8) Å	γ = 90°
Volume	1333.52(13) $Å^3$	
Z	4	
ρcalc	1.373 g/cm^3	
Absorption coefficient	0.283 mm-1	
F(000)	576	
Crystal size	0.37 × 0.21 × 0.13 mm^3	
Theta range for data collection	1.56 to 28.00°.	
Index ranges	$-5 \le h \le 5$, $-21 \le k \le 34$, $-12 \le l \le 16$	
Reflections collected	7199	
Independent reflections	3207 [R(int) = 0.0464]	
Completeness to theta = 28.00°	99.3%	
Absorption correction	None	
Refinement method	Full-matrix least-squares on F^2	
Data / restraints / parameters	3207 / 0 / 180	
Goodness-of-fit on F^2	1.015	
Final R indices [I>2sigma(I)]	R_1 = 0.0396, wR_2 = 0.0886	
R indices (all data)	R_1 = 0.0618, wR_2 = 0.0954	
Largest diff. peak and hole	0.218 and -0.368 $e.Å^{-3}$	

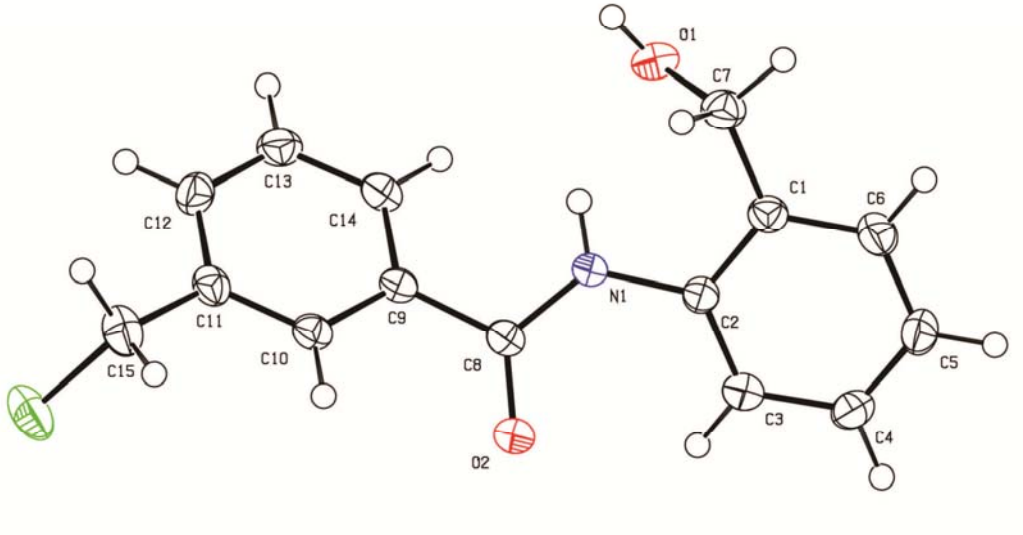

Figure S2.4.1. ORTEP diagram of 3-(chloromethyl)-*N*-[2-(hydroxymethyl)phenyl]-benzamide

Table S2.4.2. Crystal data and structure refinement for 2-[3-(chloromethyl)benzamido]benzyl 3-(chloromethyl)benzoate.

CCDC deposition code	CCDC 980628
Empirical formula	$C_{23}\ H_{19}\ Cl_2\ N\ O_3$
Formula weight	428.29
Temperature	173(2) K
Wavelength	0.71073 Å
Crystal system	Orthorhombic
Space group	*Fdd*2
Unit cell dimensions	a = 38.968(4) Å
	b = 46.919(5) Å
	c = 4.3266(3) Å
Volume	7910.6(13) $Å^3$
Z	16
ρcalc	1.438 g/cm^3
Absorption coefficient	0.354 mm^{-1}
F(000)	3552
Crystal size	0.41 × 0.04 × 0.03 mm^3
Theta range for data collection	1.36 to 27.99°.
Index ranges	$-50 \leq h \leq 34$, $-61 \leq k \leq 13$, $-5 \leq l \leq 5$
Reflections collected	7363
Independent reflections	4217 [R(int) = 0.1242]
Completeness to theta = 27.99°	98.10%
Absorption correction	None
Max. and min. transmission	0.9895 and 0.8685
Refinement method	Full-matrix least-squares on F^2
Data / restraints / parameters	4217 / 1 / 262
Goodness-of-fit on F^2	0.715
Final R indices [I>2sigma(I)]	R_1 = 0.0537, wR_2 = 0.0660
R indices (all data)	R_1 = 0.2176, wR_2 = 0.0976
Absolute structure parameter	-0.32(12)
Largest diff. peak and hole	0.260 and -0.340 e.$Å^{-3}$

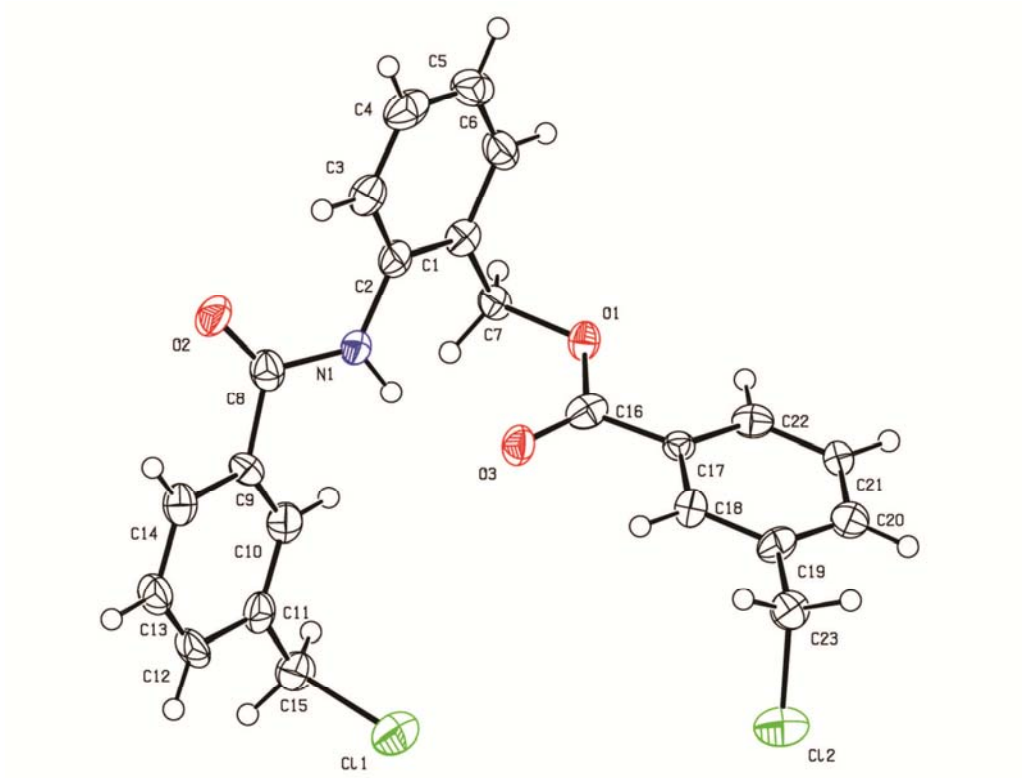

Figure S2.4.2. ORTEP diagram of 2-[3-(chloromethyl)benzamido]benzyl 3-(chloromethyl)benzoate

S2.5 TD-DFT Calculations

We provide here a brief discussion of TD-DFT calculations carried out on a model of five-coordinate DPTC-Co and it six-coordinate aqua and cyano complexes. Calculations were also performed on six-coordinate DPTC-Co complexes with a wide range of axial ligands.[12] These will be reported elsewhere. For these calculations, the *x* axis was chosen to lie along the C5–C15 vector (see Figure in Table 1 of the text), the *y* axis along the Co–C10 vector, and the *z* (axial) axis along the L_1–Co–L_2 vector.

The electronic transitions in the near UV-visible region (i.e., between 300 nm and 700 nm) as calculated by TD-DFT methods at the CAM-B3LYP/TZVP level of theory are dominated by the transfer of electron density of the frontier orbitals (HOMO – 2 to LUMO + 2) of these systems.

The HOMO – 2 to LUMO + 2 orbitals of [CN–DPTC-Co]$^-$ are shown in Figure S2.5.1. Electron density in the HOMO – 2 orbital is found in the π bonding orbitals of the pyrroles as well as in the d_{yz} metal orbital and the σ orbital of coordinated CN^-. In the HOMO – 1 orbital electron density is distributed in the π bonding orbitals of the corrole backbone, with most of the density in the "western" half on the molecule and in the d_{xz} orbital of cobalt.[¶] The HOMO orbital contains electron density distributed around the corrole backbone with a small amount of electron density found on the imidazole axial ligand and the *meso* phenyl rings. The LUMO orbital contains π bonding electron density homogeneously distributed around the corrole ring; in LUMO + 1, there is more electron density in the "eastern" quadrant. Electron density of the LUMO + 2, on the other hand, is found on the phenyl ring and amide tail of the *meso* position at C10.

Figure S2.5.2 shows the HOMO – 2 to LUMO + 2 orbitals of [H_2O–DPTC-Co]. Like LUMO + 2 of the cyanide complex, the electron density in HOMO – 2 of the aqua complex is found exclusively on the phenyl ring and amide tail of the *meso* group at the C10 position. The HOMO – 1 orbital features a homogeneous distribution of π bonding electron density around the corrole backbone. The HOMO contains electron density at the *meso* positions, pyrrole-pyrrole bridge and the pyrrolic nitrogen donors with a small amount of electron density on the metal and coordinated H_2O. In the LUMO, electron density is homogeneous distributed on the *α–β* bonds of the four pyrroles and the *meso* positions of the corrole macrocycle. The LUMO + 1 orbital features electron density at the *meso* positions

[¶] In the standard view of the corrole, the C19–C1 bond lies in the "western" quadrant, C5 in the "northern" quadrant, and C10 in the "eastern" quadrant.

and pyrrole-pyrrole bridge as well as the pyrrolic nitrogen and the α–β bonds of the pyrrole units on either side of the C10 position. Electron density is also found in the d_{z2} orbital of the cobalt ion and on both the H_2O and imidazole ligands. The majority of the electron density of the LUMO + 2 is found in an anti-bonding arrangement between the d_{z2} orbital of the cobalt and σ orbitals of the imidazole and water ligands with some density on the pyrrolic nitrogens of the inner core of the macrocycle.

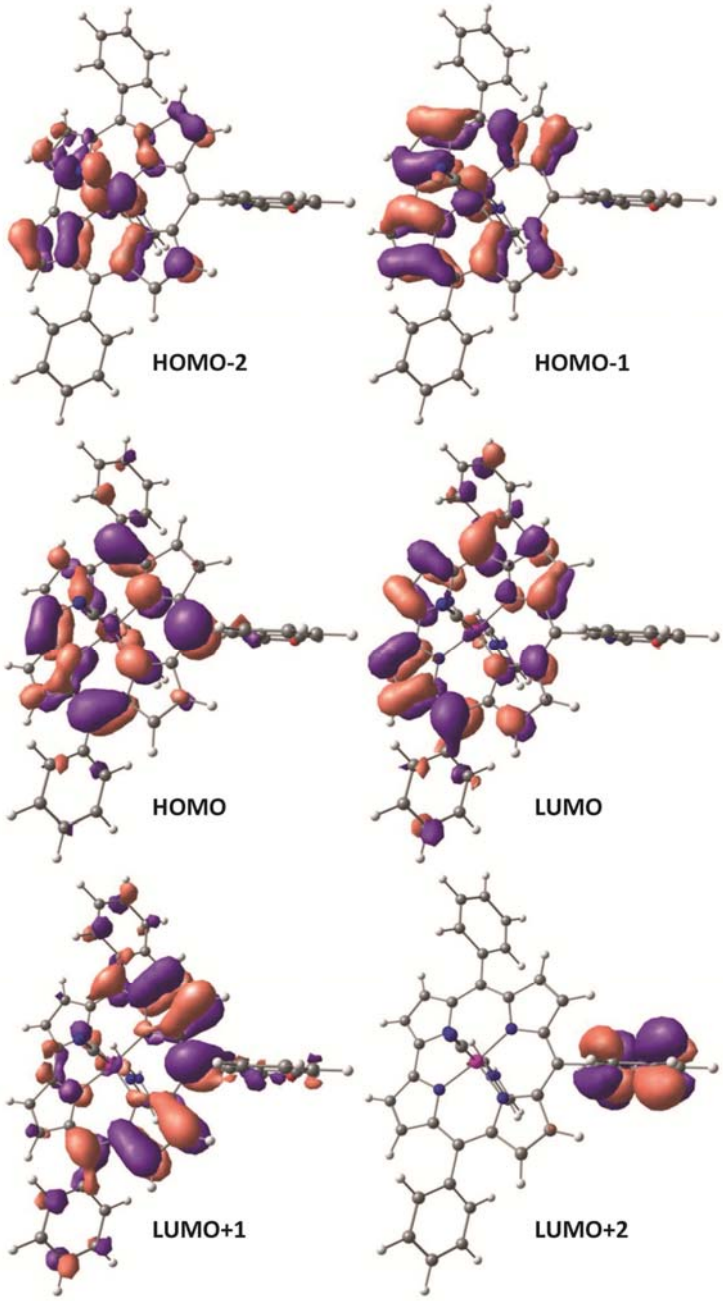

Figure S2.5.1. The HOMO – 2 to LUMO + 2 frontier orbitals of $[CN–DPTC-Co]^-$ as determined by TD-DFT methods at the CAM-B3LYP/TZVP level of theory

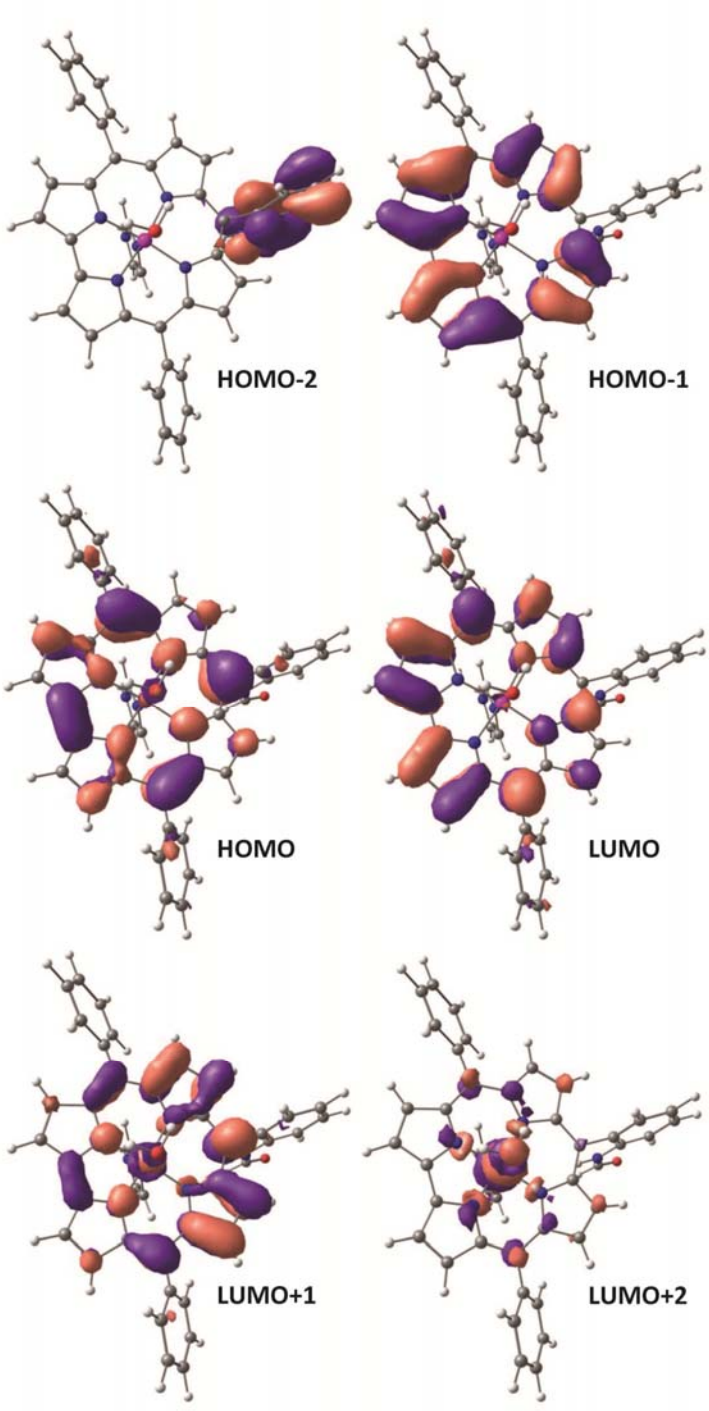

Figure S2.5.2. The HOMO – 2 to LUMO + 2 frontier orbitals of [H_2O–DPTC-Co] as determined by TD-DFT methods at the CAM-B3LYP/TZVP level of theory

The transition that gives rise to the Q band between 500 and 600 nm (see insert to Figure S6) is due predominantly to a HOMO → LUMO transition in the aqua and cyano complexes. The red shift when the axial ligand is changed from the relatively weak field H_2O to the strong field CN^- is a consequence of the decrease in the HOMO–LUMO gap. In

the case of five coordinate DPTC-Co, the Q band arises predominantly from a HOMO → LUMO + 1 transition.

According to our model of the electronic spectra of the corroles, in [H_2O–DPTC-Co], the Q band largely entails the change of electron density between orbitals on the periphery of the corrole macrocycle. In [CN–DPTC-Co]$^-$ the Q band corresponds to the transition of electron density from the inner corrole ring (atoms involved in coordination to the metal and the atoms bridging the pyrrole subunits) to the outer corrole with little involvement of the electron density on the metal or either of the axial ligands. The Q band of the five-coordinate species DPTC-Co did not arise from a HOMO → LUMO but from a HOMO → LUMO + 1 transition. The HOMO orbital of DPTC-Co contains significant Co d_{Z2} character so the transition involves not only the change of electron density on the periphery of the corrole macrocycle but also a metal → corrole charge transfer (Figure S2.5.3).

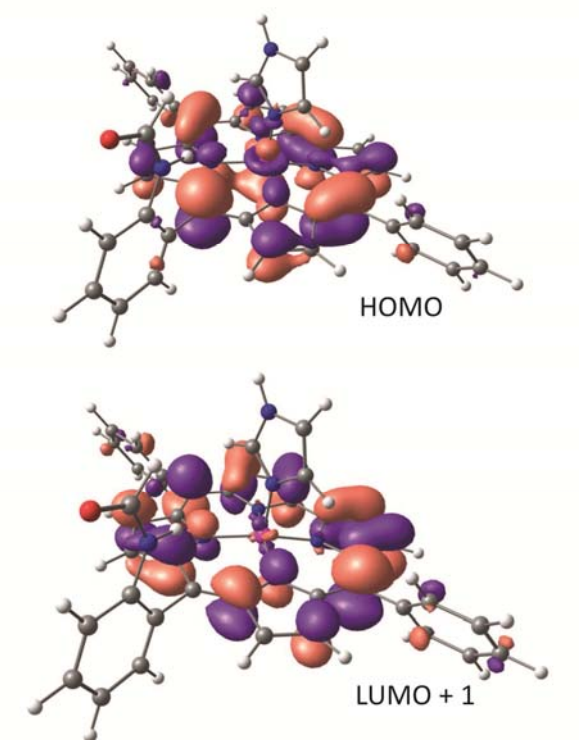

Figure S2.5.3. The HOMO and LUMO + 1 orbitals of five-coordinate DPTC-Co. The Q band in the electronic spectrum of the complex comprises largely of a transition of electron density from the HOMO to the LUMO + 1 orbital

The Soret band consists of multiple transitions (see insert to Fig. S.6), each of which is a composite of transitions between many pairs of orbitals. To help visualize the change in the distribution of electron density associated with each transition, the natural transition orbitals (NTOs)[13] of the two highest intensity transitions of the Soret band were obtained with the NAncy-Ex code[14] and are shown in Figure S2.5.4. For completeness, we also include the NTOs for the Q band although, as discussed above, the Q band is predominantly a HOMO → LUMO (or HOMO → LUMO + 1 for the five coordinate species) transition.

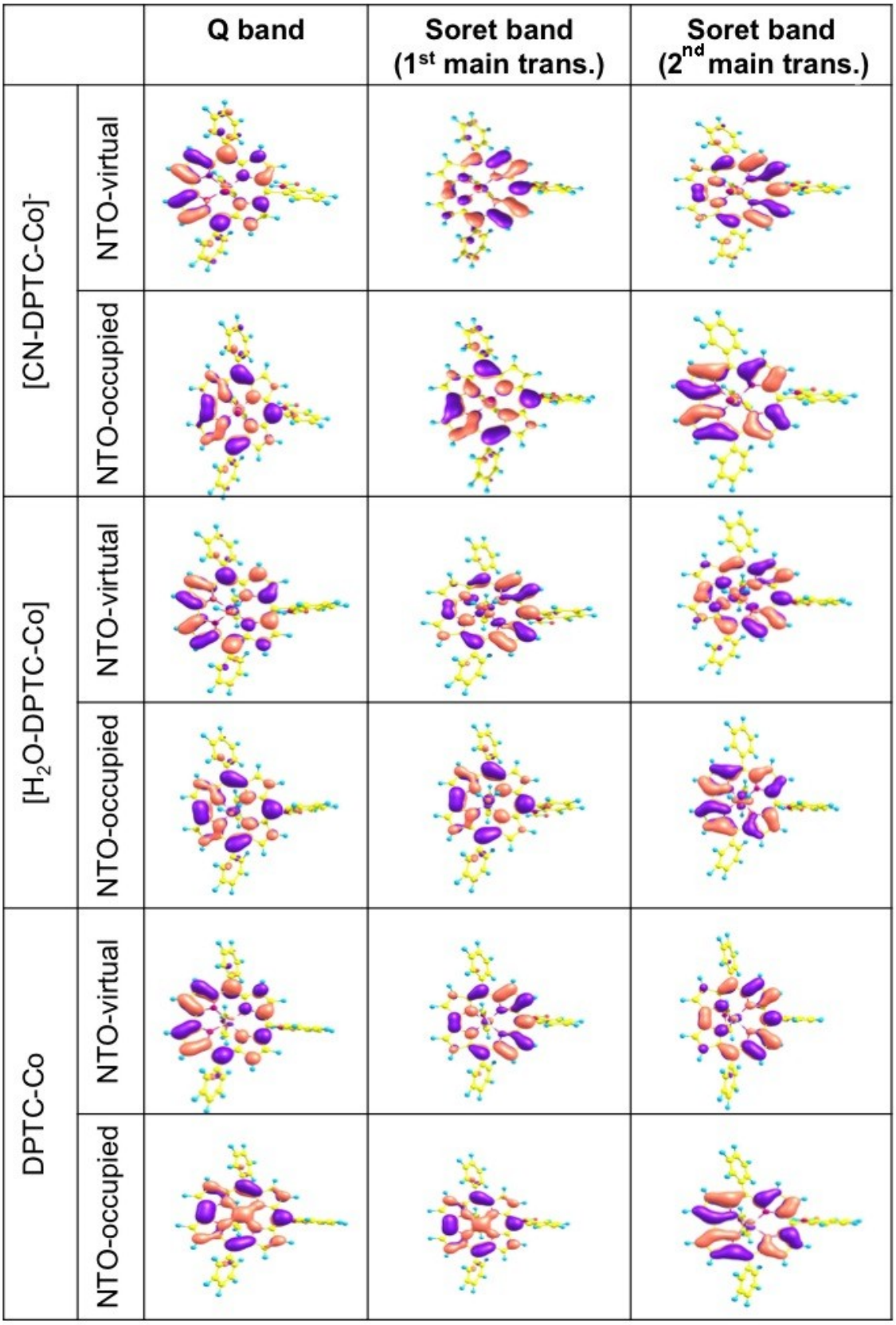

Figure S2.5.4. Natural transition orbitals (NTOs, occupied and virtual) for the principal transition of the Q band and for the two principal transitions of the Soret band as visualized by the NAncy_Ex code. Of the two highest intensity transitions in the Soret region (see insert to Fig. S6) the first main transition is the one that occurs at the longer wavelength.

As shown in Fig. 2.5.4, the transitions in the Soret region are dominated by transitions within the π system of the corrole with some involvement of electron density on the metal.

In the case of [CN–DPTC-Co]$^-$, the longer wavelength transition of the pair of principal transitions of the Soret has significant contribution from a HOMO – 1 → LUMO and a HOMO → LUMO +1 transition, while the shorter wavelength transition has significant contribution from HOMO – 1 → LUMO + 1 transition. For [H_2O–DPTC-Co], the longer wavelength transition contains significant HOMO → LUMO + 1 character, and the shorter wavelength transition is also characterized by a significant HOMO – 1 → LUMO + 1 contribution. In five-coordinate [DPTC-Co], the lower energy of the pair of Soret transitions has significant HOMO → LUMO + 2 and HOMO – 1 → LUMO + 1 character, while the higher energy transition has a major HOMO – 1 → LUMO + 2 contribution.

S3. Tables

Table S3.1. New AMBER parameters for modeling Co(III) corroles. (** = wildcard)

$$V(r^N) = \sum_{bonds} \frac{k_i}{2}(l_i - l_{i,0})^2 + \sum_{angles} \frac{k_i}{2}(\theta_i - \theta_{i,0})^2 + \sum_{torsions} \frac{V_n}{2}(1 + \cos(n\omega - \gamma))^2 + \sum_{i=1}^{N}\sum_{j=i+1}^{N}\left(4\varepsilon_{ij}\left[\left(\frac{\sigma_{ij}}{r_{ij}}\right)^{12} - \left(\frac{\sigma_{ij}}{r_{ij}}\right)^{6}\right] + \frac{q_i q_j}{4\pi\varepsilon_0 r_{ij}}\right)$$

Atom Types

Atom type	Atomic weight	Comment
co3	58.93	Co(III)
nc1	14.01	Corrole N
nc2	14.01	Corrole N
nc3	14.01	Corrole N
nc4	14.01	Corrole N
cam	12.01	*meso* carbon in corrole
cap	12.01	pyrrole carbon in corrole

Bond Stretching Parameters

Atom type 1	Atom type 2	k_i /kcal mol^{-1} Å^{-2}	l_0 /Å
co3	nc1	300.0	1.870
co3	nc2	300.0	1.870
co3	nc3	300.0	1.890
co3	nc4	300.0	1.890
nc1	cap	470.0	1.380
nc2	cap	470.0	1.380
nc3	cap	470.0	1.380
nc4	cap	470.0	1.380
cap	cap	478.0	1.410
cap	cam	478.0	1.400
cam	ca	478.0	1.490
cap	ha	344.3	1.087

Angle Bending Parameters

Atom type 1	Atom type 2	Atom type 3	k_i /kcal mol^{-1} rad^{-2}	θ_i /deg
nc1	cap	cap	70.2	108.0
nc2	cap	cap	70.2	108.0
nc3	cap	cap	70.2	108.0
nc4	cap	cap	70.2	108.0
nc1	cap	cam	70.2	119.0
nc2	cap	cam	70.2	119.0
nc3	cap	cam	70.2	119.0
nc4	cap	cam	70.2	119.0
cap	nc1	cap	67.1	108.0
cap	nc2	cap	67.1	108.0
cap	nc3	cap	67.1	108.0
cap	nc4	cap	67.1	108.0
co3	nc1	cap	31.5	126.0
co3	nc2	cap	31.5	126.0
co3	nc3	cap	31.5	126.0
co3	nc4	cap	31.5	126.0
cap	cap	cap	67.2	108.0
cap	cap	cap	67.2	108.0
cap	cap	ha	48.5	120.0
cap	cap	cam	34.0	129.0
cap	cam	cap	67.2	123.0
cap	cam	ca	67.2	118.0
cam	ca	ca	67.2	121.0
nc1	co3	nc2	30.0	81.0
nc1	co3	nc3	30.0	90.0
nc1	co3	nc4	30.0	171.0
nc3	co3	nc4	30.0	95.0
nc3	co3	nc2	30.0	185.0
nc4	co3	nc2	30.0	91.0

Torsion Parameters

Atom type 1	Atom type 2	Atom type 3	Atom type 4	½ V_n	γ	N
co3	nc1	cap	cap	4	1.2	180
co3	nc2	cap	cap	4	1.2	180
co3	nc3	cap	cap	4	1.2	180
co3	nc4	cap	cap	4	1.2	180
co3	nc1	cap	cam	4	1.2	180
co3	nc2	cap	cam	4	1.2	180
co3	nc3	cap	cam	4	1.2	180

Atom type 1	Atom type 2	Atom type 3	Atom type 4	½ V_n	γ	N
co3	nc4	cap	cam	4	1.2	180
*	co3	**	**	6	0.0	180
nc1	cap	cap	cap	4	14.5	180
nc2	cap	cap	cap	4	14.5	180
nc3	cap	cap	cap	4	14.5	180
nc4	cap	cap	cap	4	14.5	180
nc1	cap	cap	nc2	4	14.5	180
nc1	cap	cap	ha	4	14.5	180
nc2	cap	cap	ha	4	14.5	180
nc3	cap	cap	ha	4	14.5	180
nc4	cap	cap	ha	4	14.5	180
nc1	cap	cam	cap	4	14.5	180
nc2	cap	cam	cap	4	14.5	180
nc3	cap	cam	cap	4	14.5	180
nc4	cap	cam	cap	4	14.5	180
nc1	cap	cam	ca	4	14.5	180
nc2	cap	cam	ca	4	14.5	180
nc3	cap	cam	ca	4	14.5	180
nc4	cap	cam	ca	4	14.5	180
cap	cap	cap	cap	4	14.5	180
cap	cap	cap	cam	4	14.5	180
cap	cap	cam	cap	4	14.5	180
cap	nc1	cap	cap	4	1.2	180
cap	nc2	cap	cap	4	1.2	180
cap	nc3	cap	cap	4	1.2	180
cap	nc4	cap	cap	4	1.2	180
cap	nc1	cap	cam	4	1.2	180
cap	nc2	cap	cam	4	1.2	180
cap	nc3	cap	cam	4	1.2	180
cap	nc4	cap	cam	4	1.2	180
cap	cap	cap	ha	4	14.5	180
cap	cap	cam	ca	4	14.5	180
cap	cam	ca	ca	4	7.0	180
ha	cap	cap	ha	4	14.5	180
cam	cap	cap	ha	4	14.5	180
cam	ca	ca	ha	4	14.5	180
cam	ca	ca	ca	4	14.5	180

Out-of-plane bending parameters for sp^2 hybridized atoms

Atom type 1	Atom type 2	Atom type 3	Atom type 4	½ Vn	γ	N
**	**	ca	ha	1.1	180	2
**	cam	ca	**	1.1	180	2
cap	ca	cam	cap	1.1	180	2
ha	cap	cap	cap	1.1	180	2
cap	nc1	cap	cap	1.1	180	2
cap	nc2	cap	cap	1.1	180	2
cap	nc1	cap	cam	1.1	180	2
cap	nc2	cap	cam	1.1	180	2
cap	nc3	cap	cam	1.1	180	2
cap	nc4	cap	cam	1.1	180	2

Parameters for non-bonded interactions between pairs of atoms

Atom	½(min energy nuclear separation) /Å	Well depth kcal mol^{-1}
co3	2.000	0.044
nc1	1.824	0.170
nc2	1.824	0.170
nc3	1.824	0.170
nc4	1.824	0.170
cam	1.908	0.086
cap	1.908	0.086

Table S3.2. Comparison of Axial Bond Length Distances in DFT (BP86/TZVP) Models of [L–Co(N_4)–N_{ax}] Complexes[a]

L	Co–L /Å		$\Delta r_{\text{corrin-corrole}}$	$\Delta\bar{r}_{\text{corrin-corrole}}$	σ
	Corrole	Corrin	/Å	/Å	
py	1.989	2.024	0.035		
imidazole	1.961	1.985	0.024		
TMP	2.182	2.236	0.054	0.038	0.015
NO_2^-	1.945	1.966	0.021		
CH_3S^-	2.291	2.300	0.009		
CN^-	1.853	1.863	0.010	0.013	0.007

[a]N_4 = corrole or corrin, N_{ax} = imidazole (in corrole complex) or dmbzm (in corrin complex)

Table S3.3. Eigenvalues of the Hessian of the Electron Density at the Bond Critical Point of Co–L bonds, and Bond Ellipticity, in DFT Models (BP86/TZVP) in Corrole and Corrin Complexes

Corrole				
L	λ_1	λ_2	λ_3	ε
H_2O	-0.03619	-0.03497	0.34348	0.03493
py	-0.08107	-0.07447	0.53326	0.08861
imidazole	-0.07042	-0.06750	0.59713	0.04315
TMP	-0.08497	-0.08397	0.30922	0.01191
NO_2^-	**-0.11534**	**-0.10403**	0.62203	**0.10872**
CH_3S^-	-0.07539	-0.07168	0.24624	0.05175
CN^-	**-0.15423**	**-0.15385**	0.62748	0.00249
Corrin				
L	λ_1	λ_2	λ_3	ε
H_2O	-0.03647	-0.03502	0.36826	0.04137
py	-0.07894	-0.07480	0.47026	0.05537
imidazole	-0.08487	-0.08137	0.53138	0.04297
TMP	-0.07945	-0.07802	0.28283	0.01829
NO_2^-	**-0.13110**	**-0.11842**	0.56259	**0.10707**
CH_3S^-	-0.07622	-0.07290	0.23982	0.04559
CN^-	**-0.16094**	**-0.15806**	0.57315	0.01825

References

(1) Kadish, K. M.; Shao, J.; Ou, Z.; Frémond, L.; Zhan, R.; Burdet, F.; Barbe, J.-M.; Gros, C. *P.; Guilard, R. Inorg. Chem.* ***2005****, 44, 6744-6754.*

(2) Murakami, Y.; Yamada, S.; Matsuda, Y.; Sakata, K. *Bull. Chem. Soc. Jpn.* **1978**, *51*, 123-129.

(3) Guilard, R.; Jérôme, F.; Barbe, J.-M.; Gros, C. P.; Ou, Z.; Shao, J.; Fischer, J.; Weiss, R.; Kadish, K. M. *Inorg.Chem.* **2001**, *40*, 4856-4865.

(4) Guilard, R.; Gros, C. P.; Bolze, F.; Jérôme, F.; Ou, Z.; Shao, J.; Fischer, J.; Weiss, R.; Kadish, K. M. *Inorg. Chem.* **2001**, *40*, 4845-4855.

(5) Adamian, V. A.; D'Souza, F.; Licoccia, S.; Di Vona, M. L.; Tassoni, E.; Paolesse, R.; Boschi, T.; Kadish, K. M. *Inorg. Chem.* **1995**, *34*, 532-540.

(6) Kadish, K. M.; Ou, Z.; Shao, J.; Gros, C. P.; Barbe, J.-M.; Jérôme, F.; Bolze, F.; Burdet, F.; Guilard, R. *Inorg. Chem.* **2002**, *41*, 3990-4005.

(7) Licoccia, S.; Morgante, E.; Paolesse, R.; Polizio, F.; Senge, M. O.; Tondello, E.; Boshi, T. *Inorg. Chem.* **1997**, *36*, 1564-1570.

(8) Chen, P.; Ojaimi, M. E.; Gros, C. P.; Richard, P.; Barbe, J.-M.; Guilard, R.; Shen, J.; Kadish, K. M. *Inorg. Chem.* **2011**, *50*, 3479-3489.

(9) Shen, J.; Ojaimi, M. E.; Chkounda, M.; Gros, C. P.; Barbe, J.-M.; Shao, J.; Guilard, R.; Kadish, K. M. *Inorg. Chem.* **2008**, *47*, 7717-7727.

(10) Collman, J. P.; Sunderland, C. J.; Boulatov, R. *Inorg. Chem.* **2002**, *41*, 2282-2291.

(11) Berto, T. C.; Praneeth, V. K. K.; Goodrich, L. E.; Lehnert, N. *J. Am. Chem. Soc.* **2009**, *131*, 17116-17126.

(12) Zipp, C. F. PhD thesis, University of the Witwatersrand, Johannesburg, South Africa, 2013.

(13) Martin, R. L. *J. Chem. Phys.* **2003**, *118*, 4775-4777.

(14) NAncy_Ex, http://nancyex.sourceforge.net/,